ABSTRACT

Title of thesis: MODELING HETEROGENEOUS TRAFFIC WITH COOPERATIVE ADAPTIVE CRUISE CONTROL VEHICLES: A MACROSCOPIC EQUILIBRIUM APPROACH

Zachary Vander Laan, Master of Science
2017

Thesis directed by: Professor Paul Schonfeld
Department of Civil and
Environmental Engineering

This thesis proposes a modeling framework to characterize equilibrium traffic flow relations for heterogeneous traffic composed of both standard and Cooperative Adaptive Cruise Control (CACC) vehicles, capturing the impact of CACC market penetration and vehicle arrangement within a lane. The resulting parameterized fundamental diagram is then integrated with the first-order macroscopic traffic model, creating the ability to characterize operational performance on a network for heterogeneous traffic with varying CACC market penetration. This first-order approach is demonstrated through an illustrative case study which considers a small network with time-varying demand, temporary capacity reductions, and CACC market penetration ranging from 0.0 to 1.0. The results indicate that maximum throughput initially decreases as CACC traffic is introduced, but eventually improves significantly for CACC market penetration rates above 0.4. Additionally, they show that when an incident abruptly reduces road capacity,

introducing even a small fraction of CACC vehicles reduces the speed at which the congestion wavefront propagates upstream.

MODELING HETEROGENEOUS TRAFFIC WITH COOPERATIVE ADAPTIVE CRUISE CONTROL VEHICLES: A MACROSCOPIC EQUILIBRIUM APPROACH

by

Zachary Vander Laan

Thesis submitted to the Faculty of the Graduate School of the
University of Maryland, College Park in partial fulfillment
of the requirements for the degree of
Master of Science
2017

Advisory Committee:
Professor Paul Schonfeld, Chair/Advisor
Professor Ali Haghani
Professor Cinzia Cirillo

Acknowledgments

I am grateful to my advisor, Professor Paul Schonfeld, for his support and guidance during my time as a graduate student at the University of Maryland. His willingness to answer questions about the program and communicate with me was instrumental in my decision to attend UMD, and he has gone above and beyond to mentor me through the process of developing this thesis.

I would like to thank Professors Ali Haghani and Cinzia Cirillo for being part of my thesis committee and providing insightful feedback and comments.

Additionally, I am grateful for the opportunity I have had to work at the Center for Advanced Transportation Technology (CATT) for the past two years. I would like to acknowledge Tom Jacobs for giving me the opportunity to work there, and others for providing a stimulating professional environment in which to learn. In particular, I have benefited tremendously by working with and learning from Kaveh Farokhi Sadabadi and Nikola Marković.

I also want to acknowledge my family's role in this accomplishment. I am grateful for my wife, Sarah, who has lovingly supported me through this process as well as my parents, John and Lois, who made sacrifices to help give me a good education, and contributed to my enthusiasm for learning.

Finally, above all I would like to thank God for providing this opportunity and giving me the strength and support of others to complete the thesis, as well as a lifelong love for learning.

Table of Contents

List of Tables v

List of Figures vi

1 Introduction 1
- 1.1 Motivation . . . 1
- 1.2 Contributions . . . 4
- 1.3 Scope . . . 6
- 1.4 Thesis Overview . . . 7

2 Background and Literature Review 9
- 2.1 Traffic Flow Modeling Background . . . 9
  - 2.1.1 Microscopic Traffic Models . . . 9
  - 2.1.2 First-order Macroscopic Traffic Model . . . 11
  - 2.1.3 Connection between Micro and Macro Models . . . 13
- 2.2 Literature Review . . . 14
  - 2.2.1 Microscopic Perspective . . . 15
  - 2.2.2 Macroscopic Perspective . . . 20
  - 2.2.3 Discussion . . . 22

3 Modeling Equilibrium Behavior of Heterogeneous Traffic with CACC Vehicles 25
- 3.1 Overview . . . 25
- 3.2 Vehicle Classes and Behavioral Assumptions . . . 26
- 3.3 Longitudinal Control Model (LCM) . . . 28
  - 3.3.1 Microscopic Representation . . . 28
  - 3.3.2 Macroscopic Representation . . . 32
- 3.4 Characterizing S and C Behavior with the LCM . . . 33
- 3.5 Modeling Heterogeneous Traffic . . . 34
  - 3.5.1 Probabilities of Car-following Behaviors . . . 35
  - 3.5.2 Aggregate Performance . . . 37
- 3.6 Numerical Example . . . 39
- 3.7 Summary . . . 46

4 Application to Macroscopic Network Modeling 48
4.1 First-Order Continuum Traffic Model 49
4.1.1 Numerical Solution: Cell Transmission Model 49
4.1.2 Network Extension 51
4.1.3 Modeling Heterogeneous Traffic with C Vehicles 52
4.2 Case Study: Freeway Corridor 53
4.2.1 Network 53
4.2.2 Inputs 54
4.2.2.1 Time-Invariant Parameters 54
4.2.2.2 Time-Varying Parameters 56
4.2.3 Software Implementation 57
4.2.4 Results and Discussion 60

5 Conclusions 70
5.1 Extensions and Future Work 71

List of Tables

3.1 Parameter values representing car-following configurations. 34
3.2 Parameter values used for numerical example. 39

4.1 Parameter values used in macrosimulation case study. 55

List of Figures

3.1 Probabilities of S, C-S, and C-C car-following configurations. 37
3.2 Steady-state traffic flow relations for S, C-S, and C-C car-following configurations. 41
3.3 Aggregate traffic flow relations for varying proportions of CACC vehicles. 42
3.4 Aggregate traffic flow relations for varying vehicle arrangement assumptions. 44
3.5 Capacity as a function of CACC proportion for varying vehicle arrangement assumptions. 45
3.6 Capacity sensitivity to C-C response time, C-S response time, and minimum separation parameters. 46

4.1 Spatial discretization for CTM 49
4.2 Network used for case study. 54
4.3 Fundamental diagram used for case study. 55
4.4 Demand patterns at origin nodes. 56
4.5 Temporary capacity reductions representing incidents. 57
4.6 VHT at varying CACC market penetration 60
4.7 Queues at system entrance. 63
4.8 Network speeds under baseline conditions. 64
4.9 Network speeds under varying C market penetration rates. 66
4.10 Shock wave formation due to incident. 68

List of Abbreviations

x_i	vehicle i's position [ft]
$\dot{x}_i$	vehicle i's speed [ft/s]
$\ddot{x}_i$	vehicle i's acceleration [ft/s^2]
v_i	vehicle i's desired speed [ft/s]
A_i	vehicle i's maximum acceleration [ft/s^2]
S_{ij}	actual spacing between following vehicle i and leading vehicle j [ft]
S^*_{ij}	vehicle i's desired spacing between following vehicle i and leading vehicle j [ft]
b_i	vehicle i's estimate of its maximum deceleration [ft/s^2]
B_j	vehicle i's estimate of leading vehicle j's maximum deceleration [ft/s^2]
γ_i	vehicle i's aggressiveness [s^2/ft]
q	traffic flow [veh/h]
v	space mean speed [mph]
k	traffic density [veh/mi/lane]
v_f	free flow speed [mph]
l	average vehicle length [ft]
l_e	effective vehicle length [ft]
S	standard vehicle
C	CACC vehicle
q_s	S vehicle flow [vph]
q_c	C vehicle flow [vph]
p_s	proportion of S vehicles on a lane [0.0-1.0]
p_c	proportion of C vehicles on a lane [0.0-1.0]
T_s	human perception-reaction time [s]
T_c	C measurement, estimation and response time [s]
T_a	anticipative response time savings from V2V communication [s]
γ_s	human driver aggressiveness [s^2/ft]
γ_c	C aggressiveness [s^2/ft]
s_{0_s}	minimum allowable separation for S vehicles [ft]
s_{0_c}	minimum allowable separation for C vehicles [ft]
l_{avg}	average vehicle length (any type) [ft]

Chapter 1: Introduction

1.1 Motivation

Recent advances in sensing and communication technology have created an opportunity for the automotive industry to improve driver safety and convenience, with further potential to impact traffic operations and emissions. Radar, lidar, high quality imaging, and other sensor technologies are already being used to help identify vehicles and road geometry, automatically manage safe following distances, and pro-actively decelerate to avoid collisions (Lari et al., 2015). Two primary research thrusts - vehicle automation and connected vehicles - have emerged based on these advances, and are being explored in parallel by private and public sector entities.

According to the Society of Automotive Engineers (SAE) International Standard J3016, vehicles can be categorized in one of six automation levels, with level 0 representing existing fully human-driven vehicles, and level 5 describing fully autonomous vehicles that do not require human input under any conditions. In between these extremes, level 1 represents driver assist features such as Adaptive Cruise Control (ACC) or steering assistance that can manage some aspect of driving automatically (e.g., acceleration/deceleration, lane centering), while level 2

allows the vehicle to drive itself without help - although the driver is responsible for stepping in at any point if necessary. Levels 3 and 4 represent nearly and fully-autonomous vehicles, respectively, with the key difference being that drivers are theoretically required to pay attention and be able to take over if necessary in level 3 (although to a much lesser extent than level 2). Because level 4 does not require driver intervention when operating in autonomous mode, it represents the level of full automation many automotive manufacturers likely hope to attain. Finally, level 5 extends level 4 behavior to all conceivable circumstances (e.g., all terrains, off-road, etc.).

In contrast to approaches that depend on inter-vehicle communication, Autonomous Vehicle (AV) technology is self-contained, meaning it can operate in a consistent manner regardless of other vehicles' capabilities. This feature is particularly important during initial deployment when technology adoption rates are low and the majority of vehicles on the road are standard, human-driven vehicles (Mahmassani, 2016). Although some research suggests that AVs may initially enter the market as soon as 2020 with wider market penetration by 2040-2050 (Lari et al., 2015), there are still many ethical, policy and logistical hurdles that remain before their implementation is feasible (Goodall 2014; Lari et al. 2015; Fagnant and Kockelman 2015).

However, by allowing properly-equipped vehicles to communicate with one another, Connected Vehicle (CV) technology presents an approach that reduces the sensing requirements for each individual vehicle, likely lowering costs and leading to a more rapid deployment (NHTSA, 2011). CV technology is gener-

ally divided into two categories: Vehicle to Vehicle (V2V) communication, where vehicles exchange information with one other, and Vehicle to Infrastructure (V2I), where vehicles exchange information with roadside sensors (Diakaki et al., 2015). In both cases, vehicles that are equipped with standardized communication equipment - likely using a Dedicated Short Range Communication (DSRC) wireless network designed especially for this purpose (Lari et al., 2015) - can receive vital safety and operational information without needing any special sensing equipment (NHTSA, 2011). While this increases the likelihood that existing vehicles can be retrofitted to accommodate communication equipment, there are still many questions that remain to be answered, including the extent to which it can be effective, and the impact on safety and cost (Diakaki et al., 2015).

The United States Department of Transportation (USDOT) has been heavily involved in CV research, and sponsored a program to investigate many of these issues, focusing particularly on safety (NHTSA, 2011). While safety is the main impetus for autonomous and connected vehicle research, it is also important for planners and policy makers to understand the impact connected vehicles will have on traffic management and freeway operations, mobility, and the environment (Diakaki et al., 2015).

Modeling connected and automated vehicle (CAV) behavior is a relatively new research area, and the literature is not well-developed - primarily because there are few connected vehicle datasets and many of the implementation details are unknown. The expectation is that operational performance, safety, and mobility will improve (e.g., Lari et al. 2015), but results from initial studies are

subject to limiting assumptions. In particular, initial research tends to focus on purely microscopic car-following models or throughput (capacity) analysis at a macroscopic level, neglecting to characterize aggregate traffic behavior across a wide range of traffic states based on different CAV market penetration rates.

1.2 Contributions

This thesis focuses on modeling macroscopic traffic flow characteristics and aggregate performance when traffic is composed of a mix of standard and Cooperative Adaptive Cruise Control (CACC) vehicles, a technology that combines basic level 1 ACC automation with V2V communication. The main contributions of this thesis are summarized below.

- It develops a general framework for modeling mixed traffic consisting of both standard and CACC vehicles using reaction time, aggressiveness, and minimum separation parameters to quantify how standard and CACC vehicles interact. Based on the underlying car-following dynamics and possible ways standard and CACC vehicles can follow one another, it develops aggregate fundamental diagrams whose shapes are parameterized by CACC market penetration and vehicle arrangement assumptions. Thus, macroscopic equilibrium relations encapsulate underlying micro-level interactions and market penetration in a simple way, an approach which is well-suited for use in planning frameworks (e.g., first-order macroscopic traffic simulation, Dynamic Traffic Assignment).

- It analyzes how CACC vehicles impact aggregate traffic flow at various penetration rates. Based on model parameters representing realistic human driver behavior and reasonable behavioral assumptions about CACC car-following tactics, it concludes that increases in capacity do not appear until market penetration is approximately 0.4, with close to about 50% overall capacity improvement possible at 1.0. Additionally, under the assumption that CACC vehicles have less aggressive behavioral tendencies (i.e., willingness to tailgate), even a small proportion of CACC vehicles help promote a smoother transition between congested and uncongested traffic regimes.

- It integrates the heterogeneous modeling framework into a network level implementation of the Cell Transmission Model, which estimates time-dependent traffic states in a computationally efficient manner. In doing so, it connects a widely-used first-order traffic modeling approach to aggregate traffic flow relations that capture the impact of CACC vehicles. This allows a simple modeling framework to be used to for large-scale macro-level analysis without the complexity and computational expense of microscopic or higher order macroscopic traffic models.

- It presents a macroscopic traffic simulation software implementation in the Python language which incorporates CACC market penetration and parameters characterizing driver and CACC vehicle behavior.

1.3 Scope

The following items describe the scope of this thesis:

- It seeks to characterize traffic behavior at a macroscopic level, assuming that macroscopic behavior depends on steady state car-following dynamics (i.e., it does not consider lane-changing behavior).

- It focuses on two classes of vehicles: standard and CACC vehicles (CACC), and assumes that standard vehicles are characterized by human driving behavior while CACC vehicles are characterized by adaptive cruise control and sometimes V2V technology (depending on how vehicles are arranged in the traffic stream). Relative to standard vehicles, it assumes that CACC vehicles can tolerate smaller separation distance between vehicles, have lower response times that can be further improved via V2V communication when a leader-follower pair are both CACC, and exhibit more conservative car-following behavior.

- When accounting for connected vehicle dynamics, it focuses on V2V rather than V2I communication. In other words, it is concerned with modeling how car-following behavior changes when individual vehicles can communicate, not how traffic flow can be optimized through V2I communication.

- It emphasizes modeling at a high level rather than considering implementation details. That is, it avoids the electrical/computer engineering perspective that focuses on vehicle ad hoc networks, communication protocols, and

transmission details in favor of a perspective that accounts for V2V communication through logical assumptions about parameter values and the number/type of vehicles that can share information.

1.4 Thesis Overview

The rest of the thesis is organized as follows. Chapter 2 provides relevant background information on traffic modeling and a literature review of research most closely related to this thesis, including perspectives on integrating driver-assist features and V2V communication into existing microscopic and macroscopic traffic models. Chapter 3 develops a framework for modeling equilibrium car-following behavior between different combinations of leading and following vehicle pairs when traffic is composed of a mix of standard and CACC vehicles. It begins by making assumptions about standard and CACC vehicle behavior, translates these assumptions into microscopic parameter choices in the microscopic Longitudinal Control Model (LCM), parameterizes fundamental diagram curves with respect to CACC vehicle penetration rate, and illustrates the process through a numerical example. Chapter 4 demonstrates an application of this framework by integrating the aggregate traffic flow relations into a network-level Cell Transmission Model, showing how it can be used to efficiently analyze the operational impact of introducing CACC vehicles onto a network. Software is developed to perform the simulation and integrate the CACC modeling framework, and the analysis capabilities are demonstrated on a simple network with time-

varying demand and temporary capacity reductions. Finally, Chapter 5 draws conclusions from the thesis and describes future directions for research.

Chapter 2: Background and Literature Review

2.1 Traffic Flow Modeling Background

Subsequent sections of this thesis draw upon concepts from traffic flow theory, seeking to describe how standard and CACC vehicles interact when sharing the same road. Specifically, one of the goals is to describe how various pairs of standard and CACC vehicles follow each other at a microscopic level, and then consider the resulting steady-state relations from a macroscopic perspective. To provide proper context, this section briefly describes microscopic car-following and macroscopic traffic flow relations, and explain how the two are related.

2.1.1 Microscopic Traffic Models

Microscopic models consider each vehicle-driver pair to be an individual entity that makes driving decisions based on a variety of factors, including the influence of nearby vehicles and personal driving preferences (Treiber and Kesting, 2013). Microscopic models are often separated into two categories to represent the primary decisions that impact vehicle behavior: car-following and lane-changing. Car-following models describe a vehicle's longitudinal dynamics in

relation to a preceding vehicle, while lane-changing models quantify a driver's choice to leave a particular lane for a better one - perhaps motivated by improved driving conditions in a nearby lane or knowledge of an upcoming exit. Because this thesis focuses on steady state behavior, we will avoid further discussion of lane-changing models. The interested reader is directed to Treiber and Kesting (2013) and Ni (2015) for relevant chapters on modeling lane-changing behavior.

A variety of microscopic car-following models have been proposed since the 1950's, encompassing many modeling philosophies and perspectives. Popular approaches include single-regime models, which seek to describe car-following behavior for many different traffic conditions (e.g congestion, start/stop, free flow) with a single equation, as well ones that use different equations to describe separate traffic regimes (Ni, 2015). The first car-following models were single-regime stimulus response models developed by General Motors (Chandler et al., 1958), which theorized that a driver's response is a function of external stimuli and personal preference. These models express vehicle response as a differential equation that relates a vehicle's acceleration to its speed (and possibly position, depending on the formulation) with a parameter set that describes driver sensitivity. Other models, including ones proposed by Pipes (1953) and Forbes (1963), are more pragmatic than theoretical, describing the minimum spacing and headway required for safe driving, respectively. In the same vein, a more complex multi-regime model was proposed by Gipps (1981), and theorizes that drivers choose their speed such that they can stop safely even if a leading vehicle abruptly slams on its brakes. More recent literature includes the Intelligent Driver

Model (Treiber et al., 2000), which describes a following vehicle's acceleration in terms of speed and spacing, incorporating the idea of desired spacing, which is a function of driver reaction time, vehicle speed, and speed relative to the leading vehicle. Another class of car-following models is the Optimal Velocity Model (OVM), which can take many forms depending on how the optimal velocity function is specified (e.g., Bando et al. 1994, Bando et al. 1995a, Bando et al. 1995b, and Sugiyama 1999). Finally, a recent addition to the car-following model landscape is the Longitudinal Control Model (Ni et al., 2015), which seeks to unify previous models under a general framework. The LCM is used extensively in this thesis, and will be described in detail in Chapter 3.

2.1.2 First-order Macroscopic Traffic Model

In contrast to micro-level models that consider the interactions of individual vehicles, macroscopic models view traffic analogously to a fluid, characterizing it in terms of aggregate traffic states that change over time based on conservation of vehicles (similar to conservation of mass in hydrodynamics). The continuity equation is derived from vehicle conservation and describes the evolution of traffic density based on spatial flow gradients:

$$\frac{\partial k(x,t)}{\partial t} + \frac{\partial q(x,t)}{\partial x} = 0 \tag{2.1}$$

where q is the hourly vehicle flow, k is the vehicle density, and x and t represent position and time, respectively. This equation is analogous to conservation

of mass, and states that vehicles are conserved along a section of road over time, meaning that vehicles do not enter or exit the system except at system boundaries. While this continuity equation holds for all macroscopic models, the model must be closed by also specifying the flow or local speed (Treiber and Kesting, 2013). First and second-order models differ in this specification; first-order models assume a static relation between actual traffic density and the flow (or local speed), while second-order models introduce a second PDE to describe velocity dynamics.

The first-order continuum traffic flow model was first proposed by Lighthill and Whitham (1955) and Richards (1956), and is often referred to as the LWR model. It states that traffic flow is always in equilibrium with the actual density, given by:

$$q(x,t) = q_e(k(x,t)) \tag{2.2}$$

This static relation between traffic flow and density is often referred to as the fundamental diagram of traffic engineering, and is used to characterize aggregate driver behavior. Many different forms of the so called fundamental diagram have been proposed in literature based on theory and empirical observation.

For example, one overly simplistic, but often-used model for illustrative purposes is Greenshields' model (based on Greenshields et al. 1934). This model shows that at zero density (i.e. no cars on the road) traffic speeds are at the maximum free flow speed v_f, but as additional vehicles enter the road and density increases, the speed decreases linearly until it reaches the maximum density, k_{jam}.

This linear speed-density relationship implies a parabolic flow-density relationship, which is shown below.

$$v(k) = v_f(1 - \frac{k}{k_{jam}}) \tag{2.3}$$

$$q(k) = kv(\dot{k}) = v_f k - \frac{k^2}{k_{jam}} \tag{2.4}$$

Other popular models include Greenberg, Underwood, Drake, Drew, Pipes and Munjal, a discontinuous triangular model, and the Van Aerde model, which are further discussed in references such as Treiber and Kesting (2013) and Ni (2015).

2.1.3 Connection between Micro and Macro Models

Microscopic vehicle behavior can be aggregated to the macroscopic level by considering how individual vehicles behave under steady-state conditions. This equilibrium behavior implies that vehicles are not accelerating, so acceleration terms from the microscopic representation can be set to zero. Additionally, the density of a section of road is simply the inverse of the average distance headway, flow is the inverse of the average time headway, the average vehicle speed becomes the space mean speed, and macroscopic flows, density and space mean speed are related by Equation 2.2 (Treiber and Kesting, 2013).

Note that although microscopic car-following models can be transformed into steady state macroscopic equivalents, some macroscopic models do not reduce to microscopic models. That is, some macroscopic models were developed to fit empirical observations, and do not claim to be based underlying car-

following theory (e.g. Van Aerde model).

2.2 Literature Review

Existing connected and automated vehicle (CAV) research encompasses a vast array of vehicle technologies and research scopes. Vehicle technology includes AVs ranging from basic level 1 driver-assist features such as ACC (e.g., Labuhn and Chundrlik Jr 1995; Vahidi and Eskandarian 2003) and lane departure assistance (e.g., Pilutti and Ulsoy 1999; Risack et al. 2000), to fully autonomous level 4 or level 5 vehicles (e.g., Montemerlo et al. 2008; Kammel et al. 2008, Buehler et al. 2009), CVs employing V2V and/or V2I communication (e.g., Taliwal et al. 2004; Jerbi et al. 2007; Ye et al. 2008), and those which combine aspects of both automation and communication (e.g., Van Arem et al. 2006; Hu et al. 2012; Shladover et al. 2012). This paper focuses on CACC vehicles, which are human-driven ACC vehicles that leverage V2V communication. Accordingly, we primarily focus on literature pertaining to basic driver assist rather than higher levels of automation, and communication between vehicles rather than with infrastructure.

The scope of CAV research often falls into one of three categories: policy, technology, or traffic modeling. Policy-focused research helps illuminate practical, legal, and ethical issues that need to be addressed in light of CAV technology, examples of which include Goodall (2014), Fagnant and Kockelman (2015), and Kumfer and Burgess (2015). A separate body of literature focuses on the technol-

ogy itself, exploring machine vision (Pomerleau and Jochem, 1996; Subramanian et al., 2006), data assimilation algorithms to merge sensor information (Mitchell et al. 1987; Becker and Simon 2000; Hall and Llinas 2001), and connected vehicle transmission protocols (Xu et al. 2004; Jiang et al. 2006; Cheng et al. 2007). Both of these perspective are important for advancing the field, but this paper takes a traffic modeling perspective, seeking to describe how CACC vehicles impact aggregate traffic flow dynamics. Although the goal is to model steady state macroscopic behavior, there is an intrinsic connection between microscopic car-following dynamics and macroscopic aggregate behavior. Accordingly, we survey literature from both perspectives, and investigate frameworks that have been proposed to integrate mixed traffic with both standard and connected vehicles.

2.2.1 Microscopic Perspective

The microscopic modeling perspective seeks to incorporate notions of basic automation and V2V communication in mathematical expressions of vehicle-level interactions. With the goal of characterizing this technology's impact on traffic flow and stability, these micro-level characterizations are often used in microsimulation frameworks, which are particularly well-suited for modeling heterogeneous traffic consisting of multiple vehicle types (Kesting et al., 2008).

Adaptive Cruise Control (ACC) is perhaps the first driver assist feature that has the potential to significantly impact traffic flow dynamics (VanderWerf et al., 2001). While the technology is increasingly being introduced on production ve-

hicles, the market penetration is still extremely small, making it hard to directly measure the impact on traffic. Furthermore, the current implementation is primarily geared for driver comfort rather than traffic performance (Kesting et al., 2008), which creates a discrepancy between the technology's current behavior and its potential capabilities.

Initial analysis of ACC technology suggested that ACC vehicles may help improve stability and dissipate shockwaves, but did not draw clear conclusions about the impact on capacity and performance (Van Arem et al. 1996; Zwaneveld and Van Arem 1997; Yokota 1998). For example, Van Arem et al. (1996) developed a simple acceleration control strategy that incorporated both speed and distance controllers, which they used in a microsimulation framework to evaluate the impact of varying ACC market penetration. Interestingly, they found that while the presence of ACC vehicles increased stability and did not have an appreciable affect on capacity, average traffic speeds decreased at higher demand levels. More recent ACC modeling research takes a similar methodological approach; they use existing car-following models, and capture the difference between ACC and standard vehicle behavior by choosing model parameters that reflect assumptions about time and distance headways. A car-following model widely-used for this purpose is the Intelligent Driver Model, which is a highly-detailed and realistic model that parameterizes vehicles' acceleration responses in terms of maximum allowable acceleration and deceleration levels, time delay, and minimum spacing (Treiber and Kesting, 2013). Examples of ACC analyses using the IDM include Kesting et al. (2007), Kesting and Treiber (2008), Schakel et al. (2010), Horiguchi

and Oguchi (2014), and Ntousakis et al. (2015), while other car-following models such as the Optimal Velocity Model (e.g., Liang and Peng 1999; Davis 2004; Davis 2007) are also employed. Interestingly, the literature is divided when it comes to the overall impact of ACC vehicles in mixed traffic; some studies suggest positive improvements in capacity or stability (e.g., Treiber and Helbing 2001; Davis 2004), while others are less optimistic (e.g., Marsden et al. 2001). Thus, as Kesting et al. (2008) point out, the results depend significantly on the assumptions made.

From a V2V communication perspective, models capture the fact that properly-equipped CVs can exchange relevant information with other nearby CVs and use the information to inform their driving behavior. While typical car-following models express a vehicle's acceleration response in terms of variables that can be judged by a human driver (e.g., vehicle's own speed, leading vehicle's speed, separation between vehicles), models that incorporate V2V communication either explicitly or implicitly utilize information that would otherwise be unavailable in the decision-making framework.

In some cases, this involves incorporating additional information from the leading vehicle that could not otherwise be ascertained by a human driver (e.g., Li et al. (2016) propose a model which incorporates the leading vehicle's throttle position in the decision framework). In others, it simply means representing V2V communication with a deterministic rather than stochastic model. For example, Talebpour et al. (2016) model standard vehicle behavior probabilistically using prospect theory, but argue that CVs employing V2V communication are able to accurately ascertain the leading vehicle's behavior, and thus use the determin-

istic IDM to model vehicles with V2V communication. Another approach is to add extra terms to a car-following model to capture the fact that the acceleration response depends on the position/speed/acceleration of multiple vehicles. Models considering multiple forward vehicles (i.e., multi-anticipative models) include Chen et al. (2009), Chen et al. (2016) as well as Lenz et al. (1999), and Farhi (2012), which extend the Intelligent Driver Model (IDM), Optimal Velocity Model (OVM), and Linear Piecewise Model, respectively. Models which also incorporate multiple following vehicles include ones proposed by Zheng et al. (2011) and Jin et al. (2013). In both forward and rearward looking models, the literature suggests that knowledge of multiple vehicles' behavior improves local and asymptotic (string) stability as well as traffic flow capacity.

Finally, existing research has also considered both ACC and CV technology together, seeking to model the impact of both driver assist automation and V2V communication at a microscopic level. The primary example of this is Cooperative Adaptive Cruise Control (CACC), where ACC vehicles have the ability to communicate with one another via V2V communication. Accordingly, modeling efforts incorporate combinations of the ideas described above for ACC and V2V communication, respectively. Research in this area includes Van Arem et al. (2006), Nowakowski et al. (2010), Schakel et al. (2010), Shladover et al. (2012), Milanés and Shladover (2014) and Askari et al. (2016), with the majority utilizing microsimulation frameworks to draw conclusions about traffic flow. For example, Van Arem et al. (2006) model the impact of CACC vehicles by using the same MIXIC microsimulation model that was previously described for ACC

and assuming that V2V communication allows closer following distances between CACC-equipped vehicles. They focus on a lane-reduction scenario and conclude that CACC vehicles improve traffic stability and to a lesser extent efficiency. However, they also point out that the performance greatly depends on CACC vehicle penetration rate, and note that it degrades when less than 40% of the vehicle mix are CACC vehicles. Shladover et al. (2012) model a heterogeneous mixture of standard, ACC, and CACC vehicles by using a variant of Newell's linear car-following model to represent standard vehicles, and a constant time gap control policy to model ACC and CACC vehicles in a microsimulation framework. One of the main contributions they claim is obtaining realistic time-gap values for modeling CACC traffic based on field experiments. Their results indicate that ACC vehicles are unlikely to impact capacity without V2V communication, but the presence of CACC vehicles at mid to high market penetration rates produces significant improvements. From a different perspective, Milanés and Shladover (2014) use experimental results from existing ACC, CACC, and IDM controllers on production vehicles to develop a simple car-following model that selects an appropriate following-vehicle speed based on the goal of minimizing gap error. Finally, Askari et al. (2016) compare CACC traffic dynamics using three different car-following models (Gipps, Improved IDM (IIDM), and Helly), and quantify how maximum vehicle acceleration and market penetration impact maximum throughput at intersections. They conclude that the IDM is best suited for modeling CACC/ACC vehicle dynamics.

2.2.2 Macroscopic Perspective

Analysis of ACC and V2V technology from a macroscopic approach is more limited in the literature, and generally takes one of two perspectives. The first involves finding an equilibrium flow-density relation (i.e., fundamental diagram) that captures the impact of ACC and/or V2V behavior, which can then be used in the LWR model. Analytical solutions for fundamental diagrams can be obtained by transforming car-following models to their macroscopic counterparts under steady-state conditions, but these fundamental diagrams represent steady-state car-following behavior for homogeneous, not heterogeneous traffic. A small body of literature seeks to address this by proposing multi-class kinematic wave models that consider how different classes interact with one another (e.g., Wong and Wong 2002; Logghe and Immers 2008; Qian et al. 2017), but these approaches do not focus on ACC or V2V technology. While they may be applicable to the CAV domain, it is unclear whether they can capture the effects of V2V communication, where a vehicle's car-following behavior depends not only on its class, but how the vehicles are arranged. A handful of studies have analytically derived steady-state relations for heterogeneous CAV traffic, including Bose and Ioannou (2003), Levin and Boyles (2016), and Hussain et al. (2016). Bose and Ioannou (2003) start with a simple car-following relation and model mixed traffic consisting of standard and ACC vehicles by producing fundamental diagrams for 100% manual and 100% semi-automated traffic, after which they combine the two curves to form an aggregate one. From a different perspective, Hussain et al.

(2016) consider constant car-following headways at capacity conditions for different classes of CAVs, taking a probability-weighted average of these headways based on the CAV market penetration. Focusing on higher levels of automation, Levin and Boyles (2016) characterize AV behavior through improvements in reaction time in a collision-avoidance car-following model (Kometani and Sasaki, 1959), and derive a triangular fundamental diagram whose shape is parameterized by reaction time. However, rather than representing mixed traffic in a single fundamental diagram, they propose a multi-class Cell Transmission Model, which solves the LWR model numerically for multiple vehicle classes.

The second approach uses second-order models, which retain the continuity equation from Equation 4.1, but add a second PDE to describe speed dynamics as a function of density, local speed, speed changes, and non-local effects (Treiber and Kesting, 2013). A number of models have been proposed for representing ACC, including Darbha and Rajagopal (1999), Wang and Rajamani (2004), Yi and Horowitz (2006), Ngoduy (2012), and Nikolos et al. (2015). For example, Yi and Horowitz (2006) derive a second-order traffic model for ACC traffic based on the continuity equation and velocity dynamics that depend on a traffic concentration policy. However, this approach assumes that traffic is composed of 100% ACC vehicles, and thus does not consider mixed traffic. Wilson et al. (2004), Zheng et al. (2015), and Ngoduy and Jia (2016) present similar approaches, but focus in particular on modeling V2V communication with multiple leading or following vehicles. Ngoduy (2012) derives a multi-class macroscopic model for standard and ACC vehicles using the gas-kinetic-based traffic (GKT) model and adds an

acceleration term to represent ACC behavior. He finds that the presence of ACC vehicles leads to increased upstream wave speed, but that ACC vehicles help stabilize traffic and improve flows leaving a bottleneck. Building off this approach, he extends the model to also incorporate V2V communication by considering multi-anticipative effects, finding that CACC vehicles help stabilize traffic and improve equilibrium capacity relative to ACC vehicles (Ngoduy, 2013). Similarly, Nikolos et al. (2015) use the GKT model to characterize ACC and CACC traffic, but diverge from how Ngoduy models CACC vehicles by modifying the relaxation rather than convective term, and also postulating that CACC vehicles are capable of following one another at shorter time gaps. However, the model assumes that the vehicles are all ACC or CACC, without modeling heterogeneous mixtures of vehicle class. To address this, Delis et al. (2016) incorporate a penetration rate term into the formulation and perform a case study on a ring road and highway with a merge ramp, concluding that increasing CACC penetration improves both stability and capacity. However, it is unclear whether the model properly accounts for how multi-anticipative relaxation times change at low penetration rates, and further explanation would be useful to justify the penetration rate assumptions.

2.2.3 Discussion

Since connected and automated vehicles will likely share the road with standard vehicles during a phase-in period, it is important for any modeling frame-

work to be able to handle heterogeneous traffic conditions. While the heterogeneous framework can be developed with a microsimulation approach (e.g., Van Arem et al. 2006; Shladover et al. 2012), this thesis is interested in capturing the aggregate equilibrium impact of heterogeneous traffic for a large-scale planning perspective, for which the macroscopic approach is most suitable. From a macroscopic perspective, there are few existing options for modeling heterogeneous traffic flow consisting of arbitrary mixes of CACC vehicles. While a few second-order continuum models are capable of modeling CACC traffic well (e.g., Ngoduy 2013; Delis et al. 2016) and are useful for cases in which dynamic speed information is necessary (e.g., speed-harmonization), they currently have limited ability to account for heterogeneous traffic. Even as these techniques continue to mature, the second-order modeling approach characterizes vehicle dynamics at a high level of detail (i.e., incorporating anticipation, speed adaptation time, speed/density gradients, non-local effects), which requires numerical solutions that are harder to implement and calibrate relative to simpler models. Much like with microscopic approaches, this thesis is more interested in the high-level planning perspective, and seeks to quantify heterogeneous traffic in terms of steady state aggregate characteristics. From the first-order perspective, existing research either does not consider V2V communication (e.g., Bose and Ioannou 2003; Levin and Boyles 2016), or focuses only on capacity without characterizing the entire range of aggregate traffic states (e.g., Hussain et al. 2016).

Accordingly, this thesis seeks to fill the gap in the literature by proposing a methodology to model steady state, macroscopic traffic flow relations as a func-

tion of CACC market penetration. Beginning with microscopic car-following theory and physically meaningful parameters, this approach analytically develops a simple macro-level representation of these heterogeneous dynamics suitable for first-order macroscopic models without requiring microsimulation techniques or detailed second-order continuum models. Thus, it distills the complexities of CACC car-following dynamics into aggregate steady state curves, which are suitable for first-order traffic models.

Chapter 3: Modeling Equilibrium Behavior of Heterogeneous Traffic with CACC Vehicles

3.1 Overview

The goal of this section is to develop a macroscopic framework for modeling heterogeneous traffic consisting of both standard, human-driven vehicles and Cooperative Automatic Cruise Control (CACC) vehicles - which are equipped with ACC and have the ability to communicate with one another via V2V communication. We begin by qualitatively discussing their behavioral characteristics, and state assumptions that will guide the modeling process. Next, we provide an overview of the Longitudinal Control Model (LCM), which is the traffic model that will be used to represent standard and CACC driving dynamics. Employing the assumptions developed earlier, we model interactions between standard and CACC vehicles at a microscopic, individual-vehicle level and choose LCM model parameters to represent these dynamics. We then aggregate over space and time to obtain steady state macroscopic equivalent representations of these different car-following combinations (i.e., standard following standard, standard following CACC, CACC following standard, and CACC following CACC). Finally, we

discuss how to combine these relationships together to characterize overall traffic performance as a function of CACC vehicle proportion on a lane, concluding with a numerical example to illustrate the process and investigate the sensitivity of capacity to parameter choice.

3.2 Vehicle Classes and Behavioral Assumptions

The two vehicle classes considered in this study are standard vehicles (denoted S) and CACC vehicles (denoted C). S vehicles are ordinary, human-driven vehicles without adaptive cruise control or the ability to communicate with other vehicles. In contrast, C vehicles have adaptive cruise control and use sensors (e.g., radar or lidar) to measure the distance to the leading vehicle, recognize how this distance changes over time, and actuate the accelerator or brake to respond appropriately. Furthermore, this vehicle class is equipped with V2V communication, meaning that they can obtain position/speed/acceleration from the leading vehicle via DSRC (or similar communication protocol) if both the leader and follower are C vehicles. Based on these vehicle classes and the possible car-following arrangements, heterogeneous traffic consists of three types of equilibrium car-following behavior: (1) when a S vehicle follows any vehicle (S), (2) when a C vehicle follows a S Vehicle (C-S), and (3) when a C vehicle follows another C vehicle (C-C). We begin by qualitatively discussing their behavioral characteristics, and state assumptions that guide the modeling process.

- *S*: Regardless of the preceding vehicle type, S car-following behavior is char-

acterized by human factors such as perception and reaction time, following distance preference, and level of aggressiveness.

- *C-S*: When a C vehicle follows an S vehicle its acceleration response is governed by adaptive cruise control, and it cannot make use of V2V communication. Based on ACC sensor technology, we assume that the vehicle's response time (consisting of measurement, planning, and execution time) is faster than the human perception and reaction process. However, existing research suggests that ACC tends to be comfort-oriented and risk-averse, with many researchers concluding that ACC vehicles yield negligable impact on capacity in a traffic stream (e.g., Van Arem et al. 1996; Shladover et al. 2012). Thus, we describe C-S behavior as being more responsive (i.e., reacting more rapidly to stimuli), but also more conservative (i.e., less willing to follow at unsafe distances).

- *C-C*: When a C vehicle follows another C vehicle its acceleration response is still governed by ACC, but now we assume that the follower can anticipate the leader's behavior more rapidly due to V2V communication; when the leading C vehicle's estimation algorithm determines that it needs to decelerate, it communicates its intentions to the following vehicle, which allows the following vehicle to recognize that it needs to decelerate before arriving at that conclusion based on successive distance measurements. Accordingly, we assume that C-C average response time is faster than C-S.

3.3 Longitudinal Control Model (LCM)

In order to model this behavior, we turn to a recently proposed traffic model called the Longitudinal Control Model (LCM), which seeks to merge physical constraints and human behavior in a flexible, efficient way (Ni et al., 2015). On a microscopic level, the LCM is intended to be a general framework that specifies the functional form of vehicular acceleration while allowing different safety following rules - a consequence of which is that it can produce many existing car-following models. Furthermore, in steady-state conditions the model can be used to represent aggregate traffic flow relations as a function of meaningful parameters.

3.3.1 Microscopic Representation

The LCM describes a vehicle's car-following behavior in terms of the forces which act upon it. Thus, when vehicle i is following vehicle j, vehicle i's driving behavior is characterized by the overall balance in forces:

$$\sum F_i = G_i - R_i - F_{ij} \tag{3.1}$$

where

$G =$ driving force

$R =$ road resistance

$F =$ interaction force with preceding vehicle

The terms in the force balance equation are general descriptions of the different forces, but can take on various forms based on assumptions and modeling techniques. Ni presents one form of this force balance, which appears to be motivated by empirical evidence and the goal of developing an overarching unifying theory that can generalize other existing models:

$$G_i = A_i \tag{3.2}$$

$$R_i = A_i \left(\frac{\dot{x}(t)}{v_i} \right) \tag{3.3}$$

$$F_{ij} = A_i \left(e^{1 - \frac{S_{ij}(t)}{S^*_{ij}(t)}} \right) \tag{3.4}$$

yielding

$$\ddot{x}(t+\tau) = A_i \left(1 - \left(\frac{\dot{x}(t)}{v_i} \right) - e^{1 - \frac{S_{ij}(t)}{S^*_{ij}(t)}} \right) \tag{3.5}$$

where

$x_i =$ vehicle i's position [ft]

$\dot{x}_i =$ vehicle i's speed [ft/s]

$\ddot{x}_i =$ vehicle i's acceleration [ft/s^2]

$v_i =$ vehicle i's desired speed [ft/s]

$A_i =$ vehicle i's maximum acceleration [ft/s^2]

$\tau =$ time delay [sec]

$S_{ij} =$ actual spacing between following vehicle i and leading vehicle j [ft]

$S^*_{ij} =$ spacing that vehicle i desires between itself and leading vehicle j [ft]

One of the reasons why this model is so flexible is that the desired spacing rule S_{ij}^{*} can take on many different forms depending on the aspects of car-following that the modeler wants to emphasize. Ni proposes a spacing rule that allows a following vehicle to stop before hitting its predecessor given an effective vehicle length l_{e_j}, response time τ and deceleration rate that is dependent on the following driver's maximum deceleration b_i and the assumed maximum deceleration of the leading vehicle B_j. This is a slightly modified version of Gipps' model, where the vehicle of interest and its predecessor are allowed to have different deceleration values (i.e., b and B) and the velocity is assumed constant during the perception reaction time. In other words,

$$S_{ij}^{*} = l_{e_j} + \dot{x}_i\tau + \frac{\dot{x}_i^2(t)}{2b_i} - \frac{\dot{x}_j^2(t)}{2B_j} \tag{3.6}$$

where $S_{ij} >= l_{e_j}$. To understand this spacing rule, consider a leader-follower pair for which the leading vehicle may decelerate quickly at any point in time. How far should the following vehicle position itself behind the leading vehicle such that it can safely stop without causing an accident? Regardless of the speed at which the vehicles are traveling, the spacing must always be greater than the length of the preceding vehicle l_j to prevent an accident (since spacing is measured from front bumper to front bumper). Adding a small buffer (where the value depends on the comfort level of the individual driver) to the length of the leading vehicle yields the base following distance irrespective of speed: l_{e_j}. Additionally, when the leading vehicle decelerates quickly, some reaction perception time passes before the following vehicle's driver notices the tail lights, processes

the information, and presses the brake pedal. During this time, the vehicle traverses a distance of $\dot{x}_i\tau$, which is the second term in the equation. The final aspect to consider is the braking distance, which may be different for the leading and following vehicle depending on how fast they are going and the rate at which they are willing to decelerate. Thus, the last two terms capture the fact that the following vehicle estimates how much braking distance it needs relative to the leading vehicle, and (subconsciously) adds or subtracts distance to account for this. This adds behavioral realism to the model, since often times drivers do not follow at an appropriate "safe" distance such that they could stop soon enough to avoid a collision. In steady state conditions we assume both vehicles are traveling at the same speed, which implies that this safe spacing rule can be rewritten as:

$$S_{ij}^{*} = l_{e_j} + \dot{x}_i\tau + \left(\frac{1}{2b_i} - \frac{1}{2B_j}\right)\dot{x}_i^2(t) \tag{3.7}$$

$$= l_{e_j} + \dot{x}_i\tau + \gamma\dot{x}_i^2(t) \tag{3.8}$$

where γ captures the degree to which the trailing vehicle estimates they can decelerate relative to the leading vehicle. In some sense, γ captures the notion of aggressiveness, and can be used to make this safe spacing model more realistic. For example, negative values of γ imply more aggressive driver populations, which are often observed when calibrating the model based on real-world data.

In summary, the LCM microscopic formulation captures car-following behavior with the following parameters: $\{v_f, \tau_i, A_i, b_i, B_j, l_{e_j}\}$. Of particular interest is the fact that the model incorporates notions of minimum following distance,

reaction time and levels of aggressiveness, which are important concepts to consider when modeling the distinction between S and C vehicles.

3.3.2 Macroscopic Representation

Microscopic vehicle behavior can be aggregated to the macroscopic level by considering the steady-state average behavior of the vehicles. Starting with the microscopic representation, we set the acceleration equal to zero and solve for the space mean speed, noting that the spacing terms S_{ij} and S_{ij}^* become average densities k and k^* without subscripts because they represent average behavior.

$$\ddot{x}(t+\tau) = A_i \left(1 - \left(\frac{\dot{x}(t)}{v_i}\right) - e^{1-\frac{S_{ij}(t)}{S_{ij}^*(t)}}\right) \tag{3.9}$$

$$0 = \left(1 - \left(\frac{v}{v_f}\right) - e^{1-\frac{k*}{k}}\right) \tag{3.10}$$

$$v = vf\left(1 - e^{1-\frac{k*}{k}}\right) \tag{3.11}$$

The steady state ideal spacing can be found by starting with the initial formulation. After dropping the subscripts and changing individual speeds to average speeds we have:

$$S_{ij}^* = \frac{\dot{x}_i^2(t)}{2b_i} - \frac{\dot{x}_j^2(t)}{2B_j} + \dot{x}\tau + l_{e_j} \tag{3.12}$$

$$S^* = \frac{v^2}{2b} - \frac{v^2}{2B} + \tau v + l_e \tag{3.13}$$

$$= \gamma v^2 + v\tau + l_e \tag{3.14}$$

Note that S^* is a function of speed v, and represents the spacing between a vehicle and its leader that an average driver would be comfortable tolerating at a given speed. We can equivalently express this in terms of density rather than spacing:

$$k^* = \frac{1}{S^*} = \frac{1}{\gamma v^2 + \tau v + l_e} \tag{3.15}$$

Putting it all together, we can express the relationship between speed and traffic density as:

$$v = vf\left(1 - e^{1 - \frac{1}{k\gamma v^2 + \tau v + l_e}}\right)) \tag{3.16}$$

$$k = \frac{1}{(\gamma v^2 + \tau v + l_e)\left(1 - \ln\left(1 - \frac{v}{v_f}\right)\right)} \tag{3.17}$$

Finally, we express flow in terms of speed:

$$q = kv = \frac{v}{(\gamma v^2 + \tau v + l_e)\left(1 - \ln\left(1 - \frac{v}{v_f}\right)\right)} \tag{3.18}$$

Thus, macroscopic equilibrium traffic flow can be characterized with the following parameter set: $\{v_f, \tau, \gamma, l_e\}$

3.4 Characterizing S and C Behavior with the LCM

Each of the three equilibrium car-following behaviors (S, C-S, and C-C) can be described by its own LCM parameter set and Equations 3.17 and 3.18. Table 3.1 expresses these parameters in terms of the following variables:

Variable	S	C-S	C-C	Comments
Response time τ [s]	T_s	T_c	$T_c - T_a$	$0 < T_c < T_s$
Aggressiveness γ [ft^2/s]	γ_s	γ_c	γ_c	
Minimum following separation $\mathbf{s_0}$ [ft]	s_{0_s}	s_{0_c}	s_{0_c}	$s_{0_c} <= s_{0_s}$
Effective vehicle length $\mathbf{l_e}$ [ft]	$l + s_{0_s}$	$l + s_{0_c}$	$l + s_{0_c}$	
Free flow speed $\mathbf{v_0}$ [mph]	v_0	v_0	v_0	

Table 3.1: Parameter values representing car-following configurations.

$T_s =$ human perception-reaction time [s]

$T_c =$ C measurement, estimation and response time [s]

$T_a =$ anticipative response time savings from V2V communication [s]

$\gamma_s =$ human driver aggressiveness [s^2/ft]

$\gamma_c =$ C aggressiveness [s^2/ft]

$s_{0_s} =$ minimum allowable separation for S vehicles [ft]

$s_{0_c} =$ minimum allowable separation for C vehicles [ft]

$l =$ average vehicle length (any type) [ft]

3.5 Modeling Heterogeneous Traffic

Having developed a methodology for representing the possible S and C car-following relationships through the LCM, we now quantify the aggregate macroscopic traffic flow implications when both classes of vehicle are combined together on a single traffic lane. In particular, we are interested in how the steady state performance changes as demand and market penetration of C vehicles vary.

3.5.1 Probabilities of Car-following Behaviors

In order to describe aggregate steady-state traffic dynamics, we need to quantify the percentage of traffic that falls into each of the three possible equilibrium car-following categories: S, C-S, and C-C. This depends both on the overall proportion of C vehicles, as well as how C vehicles are arranged within the lane, where vehicle arrangement ranges between two extremes: randomly dispersed (i.e., representing random arrivals), and fully separated (i.e., long platoons of each vehicle type).

To do so, consider a single lane of a fixed distance that contains an arbitrary mix of S and C vehicle flows represented by q_s and q_c respectively. Define the proportion of each type of vehicle as p_s and p_c, with

$$p_s = \frac{q_s}{q_s + q_c} \tag{3.19}$$

$$p_c = \frac{q_c}{q_s + q_c} \tag{3.20}$$

First assume that C vehicles are randomly mixed with S vehicles (ie., vehicles arrive randomly). In this case the probabilities for each of the car-following configurations are given by:

$$P(S) \approx p_s(p_s) + p_s(p_c) = p_s(p_s + p_c) = p_s = (1.0 - p_c) \tag{3.21}$$

$$P(C\text{-}S) \approx p_c(p_s) = p_c(p_s) = p_c(1.0 - p_c) \tag{3.22}$$

$$P(C\text{-}C) \approx p_c(p_c) = p_c^2 \tag{3.23}$$

Next, consider how these probabilities change when the vehicle classes are di-

vided into separate platoons (which likely would require a control strategy to achieve). In this case P(S) does not change (because this configuration does not depend on the type of the leading vehicle), but the C-C configurations disappear and all become C-C (with a single possible CV-SV configuration at the platoon boundary, whose impact is negligible for large demands). Thus, the probabilities are given by:

$$P(S) \approx (1.0 - p_c) \tag{3.24}$$

$$P(C\text{-}S) \approx 0 \tag{3.25}$$

$$P(C\text{-}C) \approx p_c \tag{3.26}$$

More realistically, the vehicle arrangement will fall somewhere between these two extremes. It is unlikely that perfect separation is achievable on a single lane (at least for reasonable mixtures of S and C vehicles), even with control measures in place. Likewise, a random arrangement is somewhat unrealistic, as human drivers will likely have preferences and biases that determine who they choose to follow. Accordingly we parameterize the C-S and C-C probabilities to allow them to vary linearly between their minimum and maximum values. To do so, we introduce vehicle arrangement parameter A, where $0.0 \leq A \leq 1.0$. When $A = 0.0$, the probabilities of C-S and C-C represent randomly arranged C vehicles, while $A = 1.0$ yields probabilities representing maximum separation between classes. Using A, we rewrite the probabilities of the car-following con-

figurations as:

$$P(S) \approx (1.0 - p_c) \tag{3.27}$$

$$P(C\text{-}S) \approx p_c(1.0 - p_c)(1.0 - A) \tag{3.28}$$

$$P(C\text{-}C) \approx p_c^2 + p_c(1.0 - p_c)A \tag{3.29}$$

Figure 3.1 plots the probabilities for each of the three configurations against C proportion, repeated for different vehicle distributions (i.e., A values). As we reasoned earlier, the probability of S is independent of A, while the probability of C-S and C-C depends on how the vehicles are arranged.

3.5.2 Aggregate Performance

The aggregate behavior of traffic in a lane depends upon the weighted contribution of behavior from each of the three car-following configurations. We have already defined the probability of each car-following configuration as a

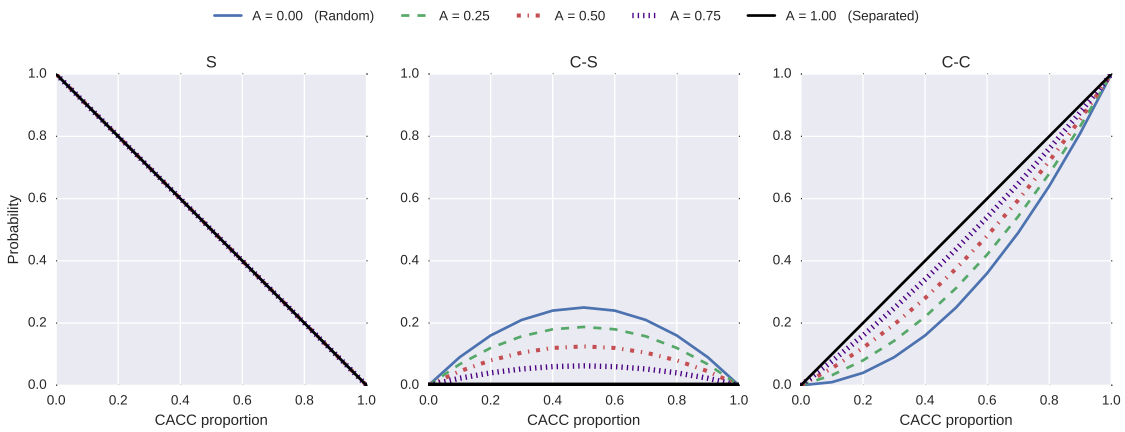

Figure 3.1: Probabilities of S, C-S, and C-C car-following configurations.

function of overall lane C proportion and a parameter that captures how the vehicles are arranged. Thus, we use these probabilities in conjunction with the LCM macroscopic relations of Equations 3.17 and 3.18 to form probability-weighted aggregate fundamental diagrams.

These equations express density and flow as a function of velocity, so every valid speed (i.e., less than or equal to free flow speed) maps to unique density and flow values (which are different for S, C-S, and C-C because they each use different parameters). To see how aggregate traffic behaves at a particular speed, a weighted average of the corresponding densities and flows of each car-following configuration are taken, with weights based on the probability of their occurrence.

Thus, the aggregate density and flow at a given speed and proportion of C vehicles are expressed as:

$$k_{agg}(v) = P(S) \cdot k_S(v) + P(C\text{-}S) \cdot k_{C\text{-}S}(v) + P(C\text{-}S) \cdot k_{C\text{-}C}(v) \tag{3.30}$$

$$q_{agg}(v) = P(S) \cdot q_S(v) + P(C\text{-}S) \cdot q_{C\text{-}S}(v) + P(C\text{-}S) \cdot q_{C\text{-}C}(v) \tag{3.31}$$

Performing these calculations across speeds on the interval $[0, v_f]$ yields aggregate flow-density, speed-density, and speed-flow curves, which capture heterogeneous dynamics in a single curve.

3.6 Numerical Example

Consider a road with a speed limit of 60 mph, and demand consisting of both S and C vehicles. Assuming that all vehicles have the same free flow speed and vehicle length, we choose the following parameters to characterize S, C-S, and C-C car-following behavior in terms of the Longitudinal Control Model: $\{v_f, \tau, \gamma, l_e\}_S = \{60$ mph, 1.2 s,$-.012$ s^2/ft, 25 ft$\}$, $\{v_f, \tau, \gamma, l_e\}_{CS} = \{60$ mph, 0.45 s, 0 s^2/ft, 23 ft$\}$, and $\{v_f, \tau, \gamma, l_e\}_{CC} = \{60$ mph, 0.2 s, 0 s^2/ft, 23 ft$\}$, which are summarized in Table 3.2. While these values are primarily selected to illustrate the methodology presented, their justification is based on the behavioral assumptions made earlier. That is, the parameters for S are first selected to characterize realistic human driver behavior (i.e., reasonable human response times, physically meaningful deceleration rates implied by the aggressiveness parameter, and resulting capacity similar to Highway Capacity Manual estimates for a 60 mph speed limit), after which C-S is chosen to represent a more responsive yet less aggressive approach that has a negligible impact on capacity. Finally, C-C captures anticipative response time savings from V2V communication by reducing the response time parameter relative to C-S. Thus, the goal of this numerical example is

Variable	**S**	**C-S**	**C-C**
Response time τ [s]	1.2	0.45	0.2
Aggressiveness γ [ft^2/s]	$-.0125$	0.0	0.0
Minimum following separation $\mathbf{s_0}$ [ft]	10	8	8
Effective vehicle length $\mathbf{l_e}$ [ft]	25	23	23
Free flow speed $\mathbf{v_0}$ [mph]	60	60	60

Table 3.2: Parameter values used for numerical example.

to provide general insight into how C market penetration affects the shape of the aggregate fundamental diagram under behavioral assumptions. Additionally, we briefly perform a sensitivity analysis to quantify how using slightly different parameter choices to differentiate ACC and V2V communication relative to S vehicles would affect capacity.

Figure 3.2 plots the following steady-state relations for each of the three car-following configurations based on the parameter sets: (a) spacing-speed, (b) speed-density, (c) flow-density, and (d) speed-flow. Plot (c) indicates that S and C-S have similar lane capacities (around 2100-2200 vph), but achieve maximum throughput at different densities. The S curve - which is characterized by human reaction times and higher levels of aggressiveness - reaches capacity at a relatively low density and has a small range of densities at which it can support near-capacity conditions, whereas the C-S curve - which is characterized by automated response and a more conservative approach - achieves capacity at higher densities and has a wider range of density at which throughput is near capacity. Furthermore, although both have similar capacities, plot (d) indicates that S achieves capacity at a higher speed than C-S. Plot (b) shows that as traffic density approaches capacity in the uncongested regime the C-S speed barely decreases (which is due to the spacing-speed relation in plot (a)), while the S speed decreases more gradually. Thus, the C-S curve achieves capacity at a lower speed, which reflects the more conservative assumption. However, when traffic density exceeds that of capacity (i.e., enters the congested regime), the performance degrades much more rapidly for S than C-S. In contrast, the C-C curve

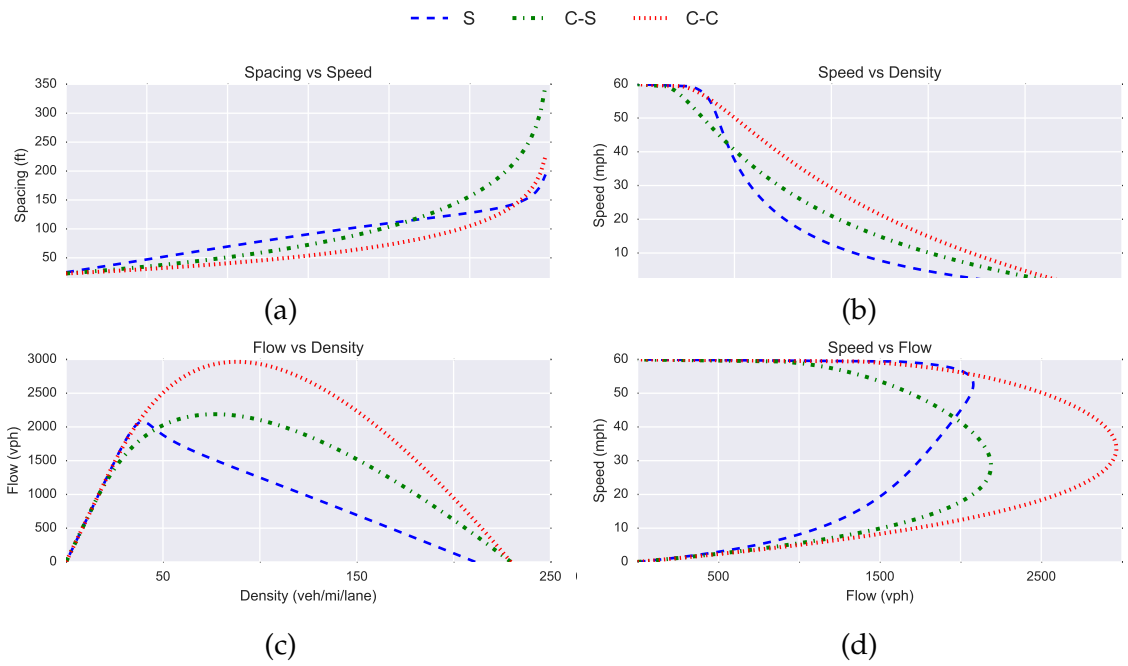

Figure 3.2: Steady-state traffic flow relations for S, C-S, and C-C car-following configurations.

has a much larger capacity (around 3000 vph), but its aggregate relations have a similar shape to C-S, reflecting fast response time and conservative tendencies. These three curves suggest that all else held constant, lower response times lead to decreased spacing for a given speed, and result in higher capacities. Likewise, increasing aggressiveness/risk tolerance can increase capacity, but also results in more rapid decrease in traffic at densities (i.e., average spacings) beyond the critical density. These results are intuitive; despite faster response times C-S does not significantly improve capacity because human drivers compensate by driving aggressively and maintaining unsafe following distances at higher speeds.

Figure 3.3 plots the following aggregate traffic flow relations for C proportions from 0.0 to 1.0 assuming a random arrival pattern: (a) flow-density, (b) speed-density, and (c) speed-flow. Note that the curves for $p_c = 0.0$ represent

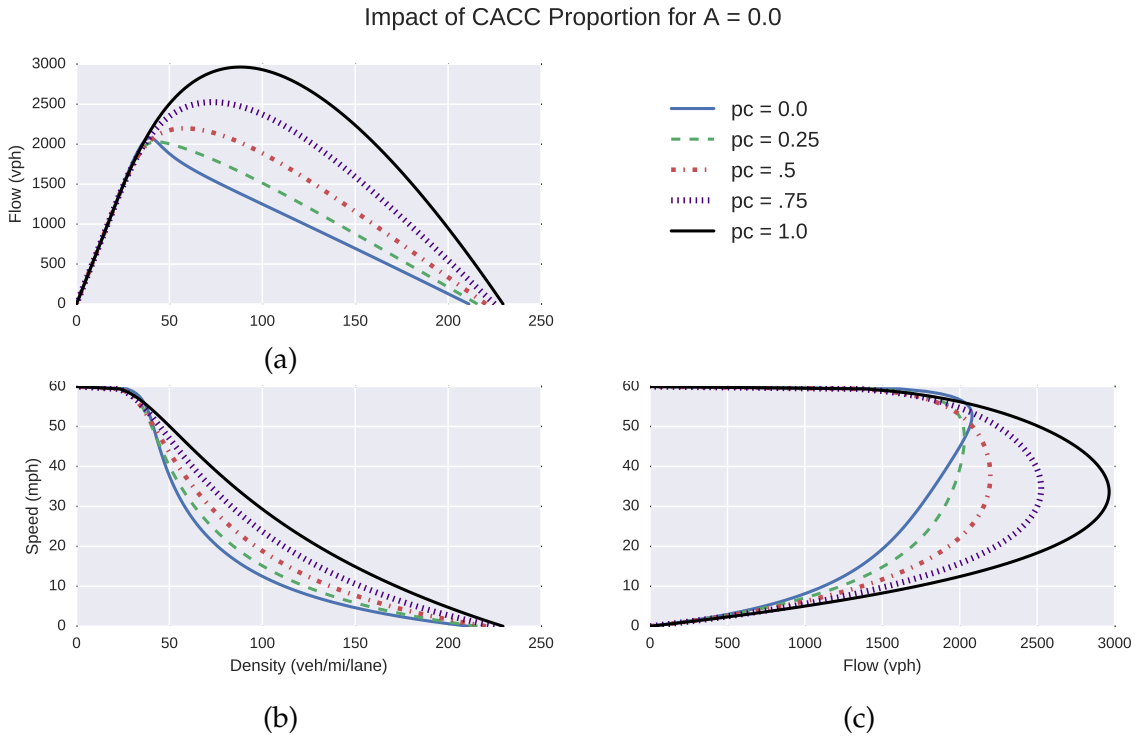

Figure 3.3: Aggregate traffic flow relations for varying proportions of CACC vehicles.

the equilibrium relations for S from Figure 3.2, while the $p_c = 1.0$ curves represent the C-C relations. In between these extremes, the shape of the curves change based on the weighted contribution of the S, C-S and C-C curves. Plots (a) and (c) highlight an interesting result: as C vehicles are introduced to a lane with all S vehicles, the capacity initially decreases before eventually increasing at high market penetration. This occurs because although S and C-S curves have similar capacities, they achieve this capacity at different speeds (as shown in the speed-flow diagram of Figure 3.2). At $p_c = 0.0$ the maximum throughput is achieved at about 52 mph because human-driven vehicles often follow closely at high speeds (i.e., exemplifying risky following behavior). As a small fraction of C vehicles are introduced to the lane, the C-S car-following behavior reduces the capacity

because despite their better reaction time, they are unwilling to follow as closely at 52 mph (since they were modeled as risk averse with γ = 0). Although C-S actually has a slightly higher capacity, it does so around 30 mph, and with only a small fraction of C vehicles on the lane their contribution is not enough to appreciably change where capacity occurs. As the C fraction continues to increase, the probability of C-C configurations increases nonlinearly, thus pulling up the overall capacity. This result is intuitive because at low C fractions there are not enough C vehicles for many C-C car-following configurations (which greatly improve performance), and the more conservative C-S driving style interferes with the aggressive manner in which standard vehicles maximize throughput.

To understand how these aggregate traffic flow relations depend on how C vehicles are arranged throughout the lane, we generate results for fixed C penetration while allowing A to range from 0.0 (random) to 1.0 (fully separated). Figure 3.4 plots the aggregate relations for multiple A values when $pc = 0.4$: (a) flow-density, (b) speed-density, and (c) speed-flow. The plots indicate that higher values of A (i.e., increased separation of vehicle classes) correspond to greater maximum throughput and similarly-shaped fundamental diagrams.

Figure 3.5 considers the relation between overall lane capacity and C penetration for a range of C distribution assumptions. As we noted in Figure 3.3, when C vehicles are randomly distributed amongst traffic, the overall capacity initially decreases at low C penetration before increasing at mid to high penetration. Given a random arrangement of C vehicles in the lane, aggregate traffic relations are primarily affected by a combination of S and C-S curves at low C

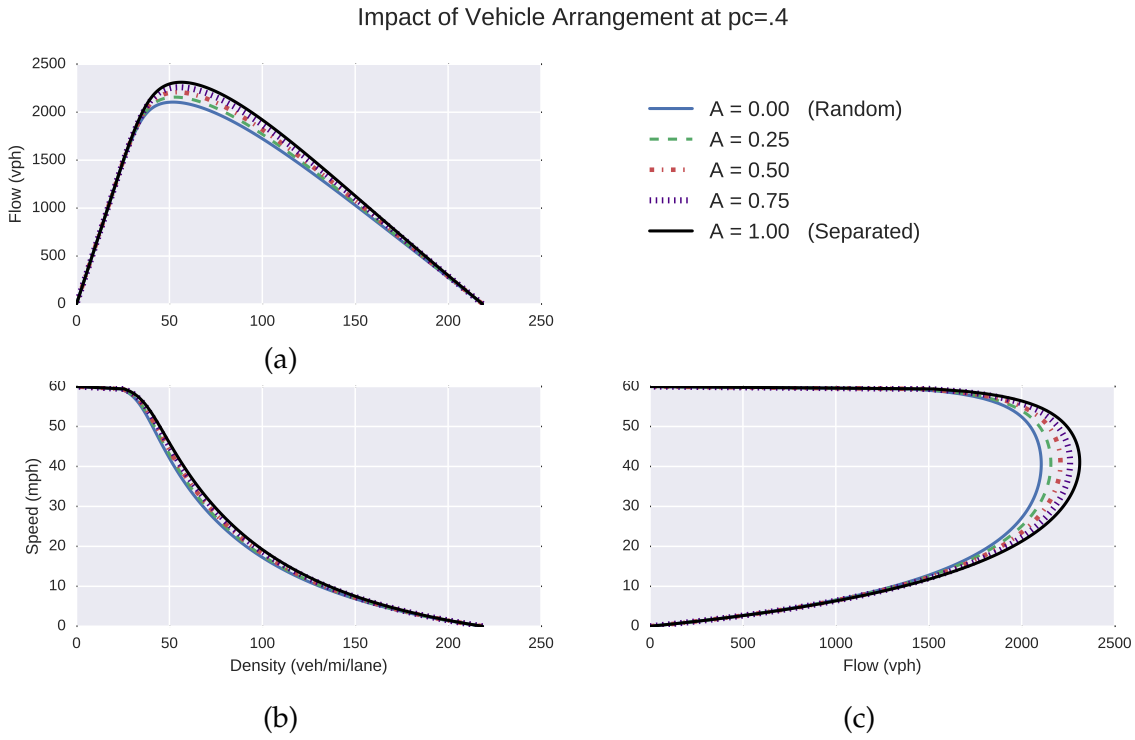

Figure 3.4: Aggregate traffic flow relations for varying vehicle arrangement assumptions.

penetrations, which explains this result. However, as C vehicles are increasingly grouped together (i.e., A increases), the aggregate composition is primarily S and C-C, which helps alleviate the initial capacity decrease for low C penetration. While this example only considers a single lane, the results suggest that it may be advantageous to separate traffic classes on multi-lane roads so that C vehicle can take advantage of V2V communication.

Finally, we consider how slightly different choices of response time and minimum separation parameters would affect capacity. Figure 3.6 plots the per-lane capacity against C proportion for (a) varying C-C response times while holding the C-S response time constant (i.e., changing anticipative time savings from V2V communication), (b) varying C-S response time while holding the antici-

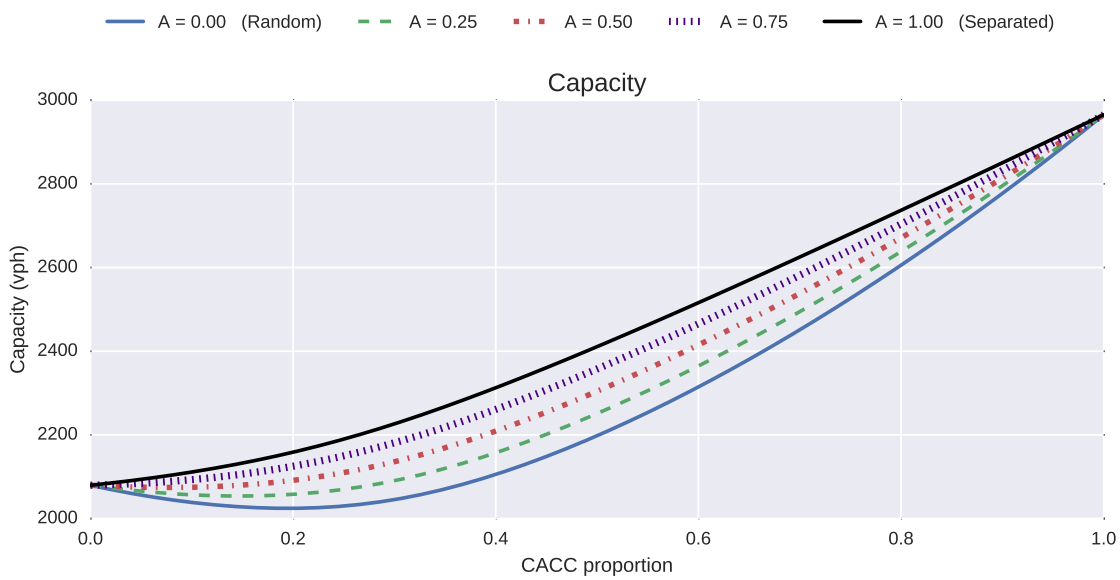

Figure 3.5: Capacity as a function of CACC proportion for varying vehicle arrangement assumptions.

pative response time savings constant (i.e., changing the impact of ACC while keeping the V2V impact constant), and (c) varying the minimum allowable separation for C vehicles. The baseline condition is indicated with a solid line in each of the plots, and perturbations about the current parameter value are considered in each direction. Plots (a) and (b) indicate that in the vicinity of the current parameter values, increasing/decreasing C-C or C-S response times by 0.1 second yields approximately 500 vph decreases/increases in capacity at 100% C market penetration, with less drastic changes at lower proportions of C vehicles. Increasing the size of the response time perturbation to 0.2 yields more drastic increases in capacity when it is lowered, and less drastic decreases when it is raised. Plot (c) suggests that the impact of minimum separation on capacity is not appreciable until market penetration reaches 50% or 60%. At 100% its effect is most pronounced, with every 1 foot increase/decrease in minimum separation

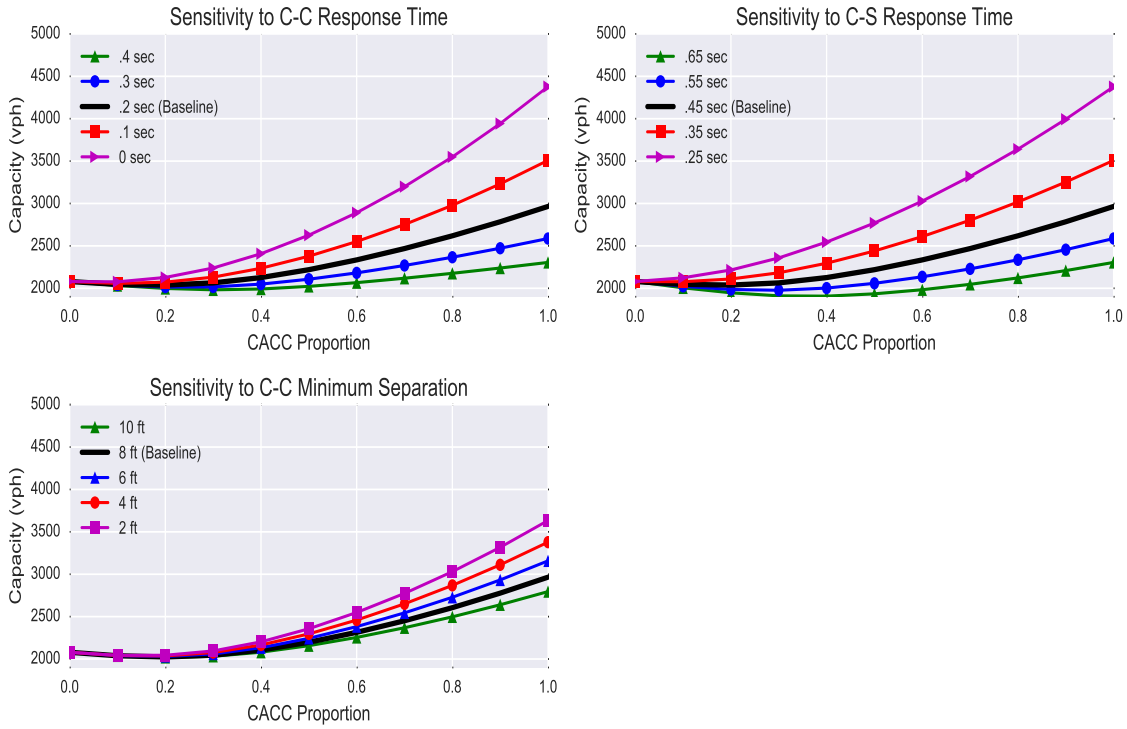

Figure 3.6: Capacity sensitivity to C-C response time, C-S response time, and minimum separation parameters.

corresponding to a 100 vph decrease/increase in capacity.

3.7 Summary

The framework proposed in this chapter allows us to model aggregate behavior of heterogeneous traffic consisting of S and C vehicles, which can be further used for analysis. Applications involve quantifying lane capacity under different C proportion and vehicle distribution assumptions, modeling operational performance on a network using the Cell Transmission Model, and evaluating policy decisions (e.g., assessing the value of implementing dedicated or managed C lanes). The numerical example in this chapter demonstrated the ability to generate equilibrium traffic flow curves and quantify lane capacity as a func-

tion of C proportion and vehicle arrangement, while the next chapter applies this framework to a multi-lane corridor.

Chapter 4: Application to Macroscopic Network Modeling

An important application of the previously-developed framework is evaluating heterogeneous traffic on a network with realistic traffic conditions. The aggregate relations developed in Chapter 3 serve as the theoretical underpinning for how heterogeneous traffic behaves, but this chapter integrates them into a larger framework that allows modeling a full range of traffic states, congestion effects, and time-varying demand. We begin by discussing the first order continuum traffic model and its numerical solution, extensions to network level-problems, and how to integrate the heterogeneous fundamental diagram in this framework. Next, we demonstrate the modeling capability by analyzing a small section of a freeway network with entrance and exit ramps, time-varying demand, and incidents that cause shockwaves to propagate along the corridor. We repeat this procedure while varying the market penetration of cooperative adaptive cruise control (C) vehicles, and draw conclusions about the impact of market penetration on overall operational performance.

4.1 First-Order Continuum Traffic Model

As described in Chapter 2, the LWR model is given by the continuity equation coupled with the assumption that traffic flow is in equilibrium with actual traffic density, given by:

$$\frac{\partial k(x,t)}{\partial t} + \frac{\partial q(x,t)}{\partial x} = 0 \tag{4.1}$$

$$q(x,t) = q_e(k(x,t)) \tag{4.2}$$

where q is the hourly vehicle flow, k is the vehicle density, and x and t represent position and time, respectively.

4.1.1 Numerical Solution: Cell Transmission Model

The LWR model is often solved numerically with a finite difference method called the Cell Transmission Model (Daganzo, 1994). To illustrate this approach, consider the road shown in Figure 4.1, which is spatially discretized into a number of smaller segments, referred to as cells. Using density as the state variable, Equation 4.1 can be discretized in space and time, yielding the following density update equation for cell i:

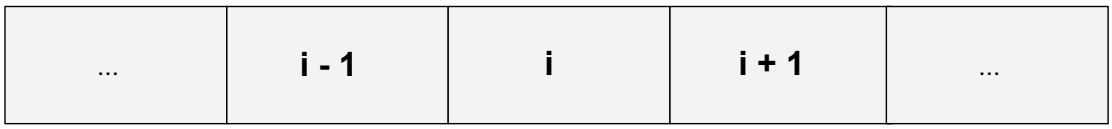

Figure 4.1: Spatial discretization for CTM

$$k_{t+1}^{i} = k_t^i + \frac{T}{L}\left[Q_t^{up} - Q_t^{down}\right] \tag{4.3}$$

where:

k_t = traffic density on the cell at time t [veh/mi/lane]

T = constant time step between iterations [s]

L = cell length [mi]

$Q_t^{up} = Q_t(k_t^{i-1}, k_t^i)$ = flow rate at the upstream cell boundary at time t [veh/hr]

$Q_t^{down} = Q_t(k_t^i, k_t^{i+1})$ = flow rate at the downstream cell boundary at time t [veh/hr]

The flux equation $Q(a, b)$ is used to calculate the flow rate between adjacent cells based on the following supply/demand rules for upstream cell with density a and downstream cell with density b.

$$Q_t(a, b) = \min\{D_t(a), S_t(b)\} \tag{4.4}$$

where $D_t(a)$ is the flow demanded by the upstream cell at time t, and $S_t(b)$ is the flow supplied by the downstream cell at time t. These supply/demand functions are defined by:

$$D_t(a) = \begin{cases} q(a) & a \leq k_{crit} \\ q(k_{crit}) & a > k_{crit} \end{cases} \tag{4.5}$$

$$S_t(b) = \begin{cases} q(k_{crit}) & b \leq k_{crit} \\ q(b) & b > k_{crit} \end{cases} \tag{4.6}$$

These rules show that the flux function depends on both the equilibrium flow-density relation of both upstream and downstream cells.

Additionally, note that the choice of L and T must satisfy the CFL condition (Courant et al., 1967) to maintain numerical stability:

$$\frac{T \cdot v_f}{L} \leq 1.0 \tag{4.7}$$

This numerical stability condition ensures that vehicles traveling at speeds up to and including v_f cannot pass through an entire cell in a single iteration.

To summarize the CTM: at discrete time intervals, each cell is updated to reflect the new traffic state that is a result of the previous state and any changes that occurred during the most recent time step, with flux rules at the cell boundaries controlling the number of vehicles that can pass between cells.

4.1.2 Network Extension

The LWR model and CTM numerical solution can be extended to more complex networks with merging/diverging behavior, but the flux rules that govern the amount of flow that may pass through cell boundaries are more complicated

because they have to account for the various possible geometries. Thus, the CTM update equation, Eq. 4.3, remains the same, but Q_t^{up} and Q_t^{down} are dependent on the network structure.

A modeling perspective described by Papageorgiou et al. (2010) uses a directed weighted-graph structure to represent the road network, with nodes representing sources, sinks, and points of discontinuity, and links connecting the nodes in the direction of travel, representing road segments and entrance/exit ramps. Since links can be arbitrarily long depending on the road geometry, they are often broken into smaller, equal sized segments called cells. These cells form the spatial structure for macroscopic traffic modeling, and are characterized by temporally varying traffic density as defined by the CTM. Note that a common simplification is to assume that only two links may enter or exit any given node, which reduces the complexity of the flux rule logic that governs the CTM solution.

4.1.3 Modeling Heterogeneous Traffic with C Vehicles

The first order macroscopic traffic model admits a generic equilibrium q-k relation, which is subsequently used in the Cell Transmission Model flux equation. Thus, C traffic can be incorporated into this framework by using an aggregate q-k curve developed from the methodology presented in Chapter 3.

4.2 Case Study: Freeway Corridor

In order to illustrate the fact that this framework can be used to analyze complex traffic conditions, this case study models a simple network with merging/diverging behavior, time-varying demand at the entrances and multiple incidents. In addition to demonstrating the modeling capability, the goal is to quantify the network operational performance by varying C vehicle market penetration between 0.0 and 1.0.

The road network is represented by a directed graph, where the links are spatially discretized into cells that are approximately 0.25 miles long. Based on 10 second update time steps, the Cell Transmission Model (Eq 4.3) is used to characterize the traffic state evolution over the course of a two hour simulation time period based on an exogenously specified market penetration rate of C vehicles.

4.2.1 Network

The simple network used for this case study is shown in Figure 4.2, and consists of a six mile corridor with four lanes in each direction, and has two origins, and two destinations. The network is divided into seven corridor links, each of which is discretized further into approximately .25 mile cells that provide a fine level of spatial resolution.

4.2.2 Inputs

The model inputs include time-invariant fundamental diagrams (and corresponding link parameters), and time-varying demand, split ratios, and incident occurrences.

4.2.2.1 Time-Invariant Parameters

The parameters summarized in Table 4.1 are used to describe human and C car-following behavior along the network. As described in Chapter 3, these parameters form the basis for developing the aggregate fundamental diagram as a function of C market penetration. Once the fundamental diagram is constructed, it can be used to obtain macroscopic parameters that are utilized in the simulation: capacity, critical density, and jam density.

Theoretically these fundamental diagrams could vary across the network (i.e., each link's fundamental diagram may be obtained from different underlying parameters) but we assume that this network is characterized by constant geometry and driver behavior. Thus, we assume that each link uses the same fundamental diagram, which is shown in Figure 4.3 for five different C market

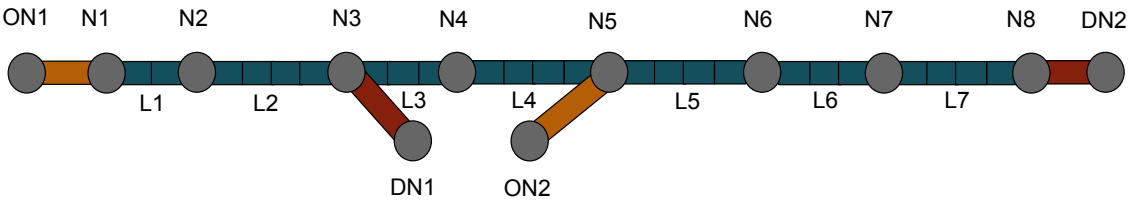

Figure 4.2: Network used for case study.

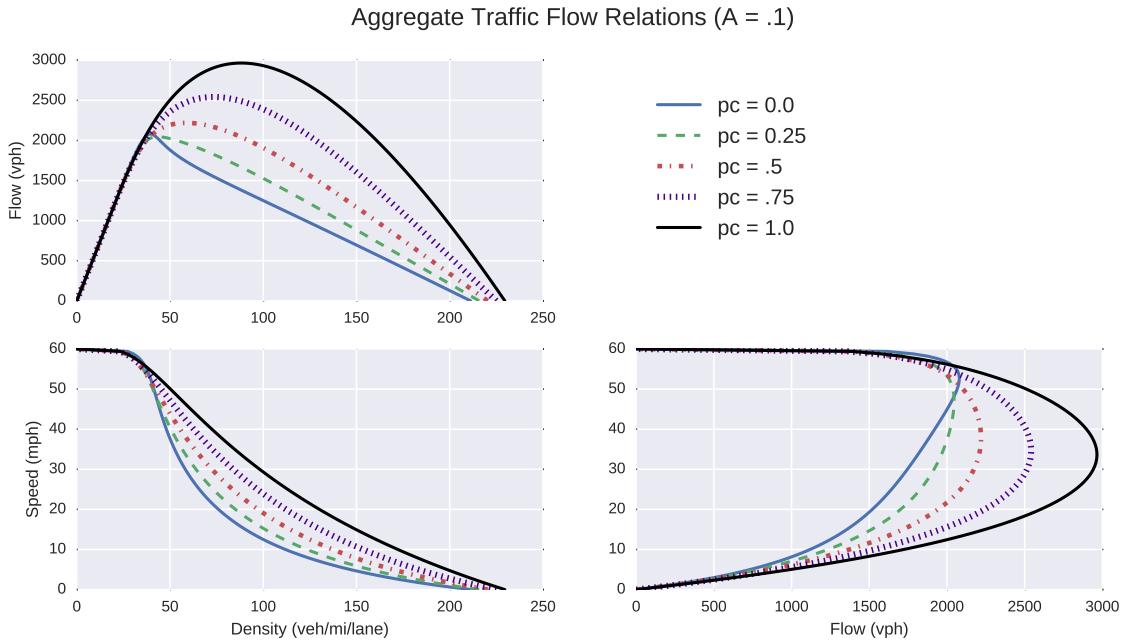

Figure 4.3: Fundamental diagram used for case study.

penetration rates. Note that these fundamental diagrams are based on the assumption that vehicle traffic is nearly randomly distributed in each lane. To account for slight driver biases we use A = 0.1 (where A ranges from 0.0 to 1.0, with 0.0 representing a random arrangement and 1.0 representing maximum separation between vehicle classes).

Variable	**S**	**C-S**	**C-C**
Response time τ [s]	1.2	0.45	0.2
Aggressiveness γ [ft^2/s]	$-.0125$	0.0	0.0
Minimum following separation $\mathbf{s_0}$ [ft]	10	8	8
Effective vehicle length $\mathbf{l_e}$ [ft]	25	23	23
Free flow speed $\mathbf{v_0}$ [mph]	60	60	60

Table 4.1: Parameter values used in macrosimulation case study.

4.2.2.2 Time-Varying Parameters

Demand

Vehicle demand originates from two origin nodes: ON1 and ON2, which are connected to the corridor through origin links (ON1, N1) and (ON2, N5). The two hour simulation is divided into 8 fifteen minute time periods, during which demand at ON1 and ON2 can take on different values. In order to account for times at which demand exceeds capacity, we model the origin links as having infinite storage capacity, and use a simple queueing model to keep track of time spent waiting to enter the network.

Split ratios

Like demand, the split ratios (i.e., the ratio of vehicles taking each possible path at a diverging node) can vary over the course of the simulation. Here the only split ratio of interest occurs at node N3, where a percentage of vehicle demand exits to destination node DN1 and the rest continues along the corridor. For the sake of simplicity we assume that this value remains constant over the course of the

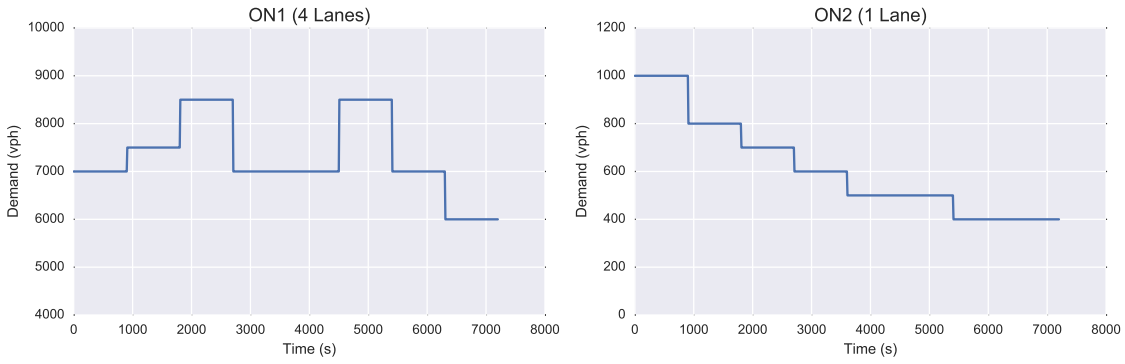

Figure 4.4: Demand patterns at origin nodes.

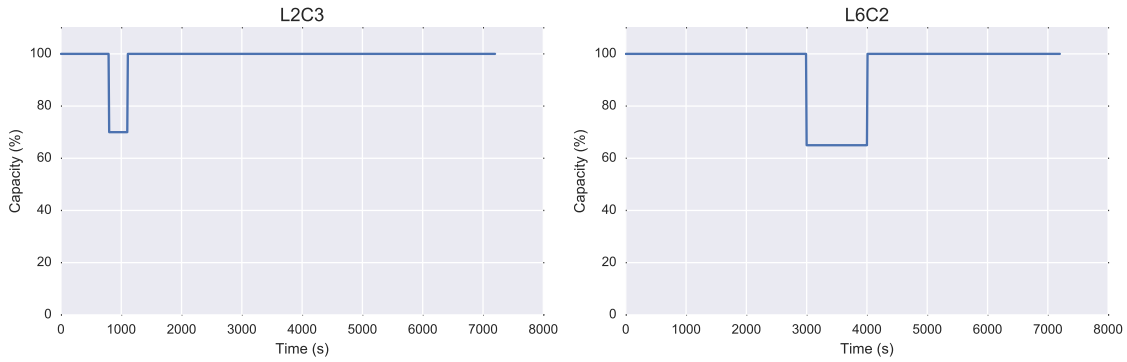

Figure 4.5: Temporary capacity reductions representing incidents.

simulation, with 10% of traffic demand exiting at N3. Thus, although we assume constant split ratios, we categorize split ratios as time-varying because in general they will likely change over the course of a day.

Incidents

In order to create interesting congestion patterns, we introduce two incidents over the course of the simulation time period. To do so, we reduce link capacity of two cells at different points during the simulation. These capacity reductions are illustrated in Figure 4.5, which shows capacity reductions of 30% and 35% for 300 and 1000 seconds at cells on links 2 and 6, respectively.

4.2.3 Software Implementation

The simulation logic described above was implemented in Python as a standalone program. The design approach was to develop a modular, object-oriented software library capable of performing analysis on arbitrary networks using any fundamental diagram, user-defined demand patterns, etc.

The basic usage involves providing inputs via appropriately-formatted csv

and json files detailing network geometry, demand, split ratios, incidents, fundamental diagram parameters, and various user options to control simulation time, time step size, output options, etc. This usage allows the user to run a simulation based on pre-specified inputs without interacting with the results until it is done.

The second, more advanced mode involves interacting with the simulation programmatically. This approach allows the user more control over simulation inputs, and is designed with real-time estimation applications in mind. For example, rather than providing the simulation with a description of how demand changes over an extended period of time based on historical data, the user can estimate traffic states for a single timestep (representing the immediate future), and use the results in a data assimilation framework.

On a high level, the program works by building a directed graph to manage the relationships between the nodes (origins, destinations, points of discontinuity, etc.) and links (road segments that are further divided into equal-length cells), and then iterating through all of the cells in the network and updating the traffic states based on the CTM update equation. The update equation depends on the cell's fundamental diagram, demand levels, split ratios, incidents, and the road geometry - which characterizes how the flux rules are applied (i.e., whether to consider merging/diverging junctions). To do so, it relies on the following classes, which are briefly summarized here:

- *InputManager*: Manages the configuration options (e.g., simulation duration, iteration time step, fundamental diagram type), reads configuration

files if necessary, creates input data structures, and provides basic error-checking.

- *FundamentalDiagram*: Constructs aggregate traffic flow relations based on input parameters and the fundamental diagram type, and provides methods to return speed and flow as a function of traffic density.

- *Network*: Models the road network as a directed graph, and provides methods to answer relevant queries about nearby road segments (e.g., is a particular link the only one entering the downstream node from the same direction, or is there also another merging link?). Internally this class uses the Python graph theory library, iGraph.

- *Simulation* Runs the simulation for the specified time period using the configuration dictated by InputManager. This class does not perform the traffic state updates, but accesses the results at each iteration and keeps track of them for later analysis.

- *Macroscopic Traffic Model* This class is responsible for performing the traffic state update for all cells on the network. It makes use of generic classes to avoid overly-specific implementation details (e.g., it uses the FundamentalDiagram class to map density values to speeds or flows without worrying about whether the underlying fundamental diagram is Greenshields, Triangular, LCM, etc) and implements the core logic. As each cell is updated, it uses the Network class to figure out whether the upstream and down-

stream cell boundaries involve merging/diverging links, and accounts for this when implementing the flux rules.

- *Results* Organizes and formats the simulation results so that they can be printed to the console or written to csv files.

- *Analysis* Provides methods to answer questions about the results. For example, using trajectory reconstruction, it can calculate the time-dependent travel time along different paths.

4.2.4 Results and Discussion

Figure 4.6 plots Vehicle Hours Traveled (VHT) against C market penetration, showing how total time in the system responds to incremental changes in the mix of standard and C vehicles as the demand patterns and other inputs remain unchanged. Figure 4.6 shows two measures of vehicle-hours: one on the

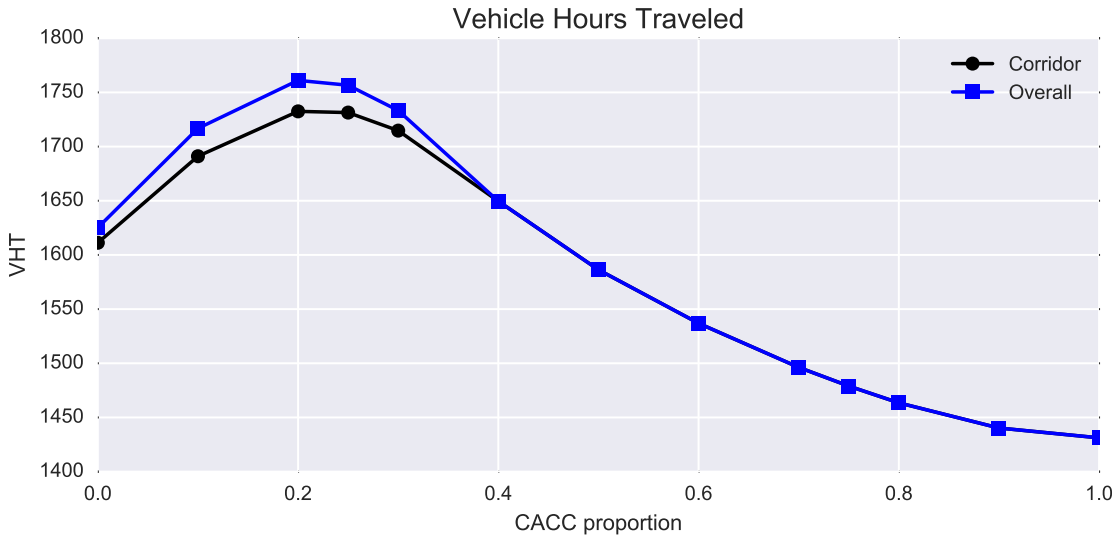

Figure 4.6: VHT at varying CACC market penetration

corridor itself, and the other accounting for time spent waiting to enter the facility. The curves indicate that VHT increases as C vehicles are initially introduced on the network, and continues to rise until C market penetration reaches about 0.2, after which it decreases the rest of the way, reaching the baseline VHT level between 0.3 and 0.4. To explain these plots, it helps to recognize the total number of vehicles entering the system is constant across all scenarios (because the input demand is the same for all market penetrations of C vehicles), so the shape of the VHT curves depends only on how long vehicles spend in this system. Consequently, there are two reasons why the average time spent in the system changes as C market penetration increases. First, recall from Figure 3.3 that capacity initially decreases as C vehicles are introduced at low penetration rates; capacity drops from 8318 vph at $p_c = 0.0$ to 8151 vph at $p_c = 0.2$ for a loss of 167 vph. The demand levels for most of the simulation are 8000 vph or less, but there are two 15 minute time periods during which demand reaches 8500 vph, which exceeds capacity for low market penetration levels. During these 30 minutes, the vehicles that are unable to enter the facility form a queue at the system entrance, which grows faster for the case when market penetration is around 0.1-0.3 because demand exceeds capacity by a larger margin than the baseline condition. Thus, the VHT curve can be partially explained by capacity initially decreasing as C vehicles are introduced. The second contributing factor is that standard vehicles (i.e., $p_c = 0.0$) achieve maximum throughput at a higher speed than when C vehicles are introduced (reflecting assumptions about human driver aggressiveness). For market penetrations where $0.0 \leq p_c \leq 0.33$ the capacity is slightly larger than

8000 vph, which means the system operates just below capacity for much of the simulation (based on the specified demand levels). Under these conditions, the standard vehicle-only traffic is able to pass through the system at a higher speed than when a low percentage of C vehicles with less aggressive tendencies are mixed into the traffic stream. As market penetration increases beyond $p_c = 0.33$, the capacity increases, which both reduces queuing delay at the entrance and also means traffic operates farther away from capacity, thus increasing the speed and reducing VHT.

Based on this explanation, we would expect queues to form at the system entrance (i.e., demand originating from node ON1 at origin link OL1) during the two 15 time periods when demand exceed capacity, with the queue length greatest when capacity is the lowest: $p_c = 0.2$. Note that demand is much lower at the entrance ramp (i.e., demand originating from node ON2 at origin link OL2) and is aways accommodated on the network, meaning that queues never form there. Figure 4.7 plots the queues at the system entrance only for low C market-penetration rates, because no queues form once p_c exceeds 0.4.

Having investigated the aggregate network performance, we now turn our attention to Figure 4.8, which shows the time-varying space-mean speed at every cell along the main corridor for the baseline scenario in which $p_c = 0.0$. The y-axis represents the distance along the main corridor, with each cell equaling approximately a quarter mile, while the x-axis represents time at 10 second time intervals. This level of granularity helps visually highlight how speed changes propagate through the corridor, which is particularly useful when investigating

the impact of incidents. First, notice that vehicles travel through the system beginning at the origin, with trajectories moving up and to the right (i.e., through space and time) at a slope given by the speed.

Ignoring the two congestion patterns for now, note that changes in input demand at the system entrance can be seen by the diagonal bands of equal color (i.e., equal speeds) that extend the length of the corridor and change every 15-30 minutes (matching the times at which the input demand curve steps to a new value). The bands are diagonal because it takes time for changes in demand at the system entrance to travel the length of the corridor and impact average speed downstream. Another feature that stands out is the horizontal band that encompasses the cells on links 3 and 4, and generally indicates higher speeds than up or downstream. This is due to the fact that there is an exit ramp immediately before the first cell on link 3, and 10% of traffic diverges, with only 90% contin-

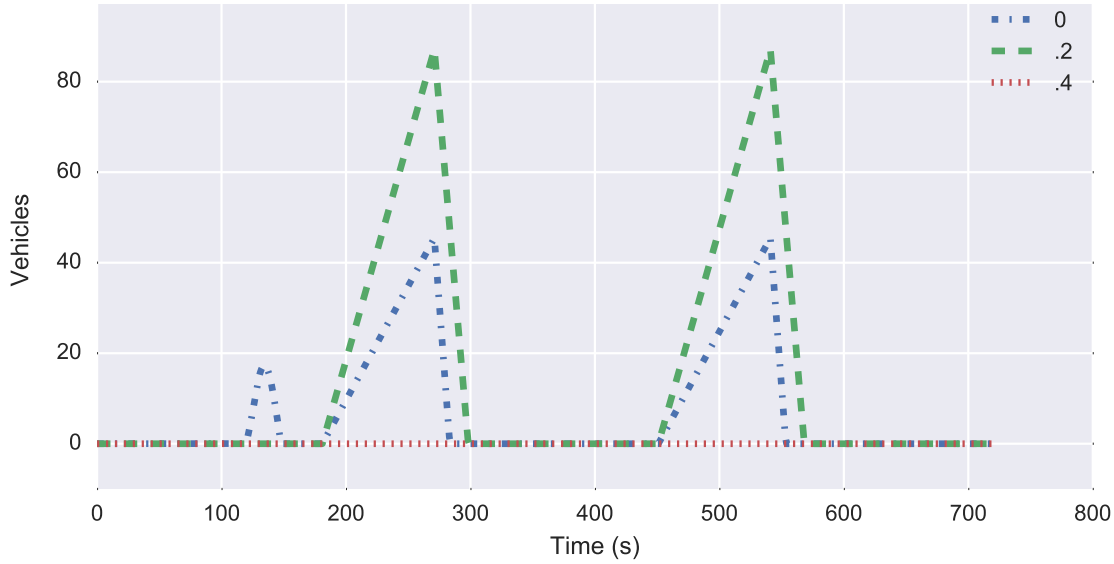

Figure 4.7: Queues at system entrance.

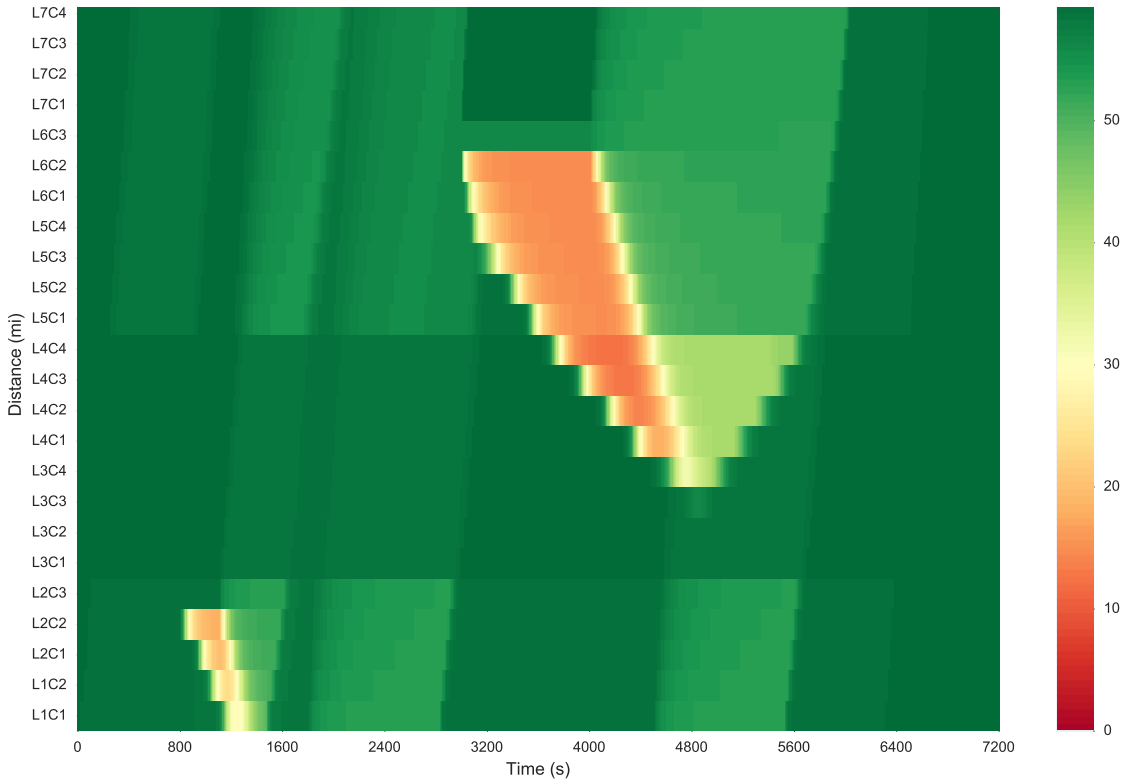

Figure 4.8: Network speeds under baseline conditions.

uing on the main corridor, thus increasing the speed in this section. Similarly, there is an entrance ramp directly after link 4, which means that any flow on subsequent links has to come from a combination of link 4 and the entrance ramp OL2. If traffic is not congested on links 4 and 5, the speed on link 4 will be greater than link 5 because it has less vehicles traveling on it (due to the merging link), which explains the change in speed seen at the boundaries between links 4 and 5. However, if link 4 enters a congested state, the merge link entering the same downstream node may hamper its ability to send the maximum flow to try to dissipate the congestion.

Now consider the congestion patterns, focusing in particular on the incident taking place on cell 3 of link 6 between t = 3000 and 4000 sec, characterized

by a 35% capacity reduction during this time period. At t = 3000 sec the flow on link 6 is 8090 vph, which represents a traffic state near capacity. When capacity is reduced from 8318 vph to 5406 vph at L6C3, the upstream cell's density (i.e., L6C2) quickly enters a congested state because its outflow is limited to 5406 vph, while flow continues to enter at 8090 vph. As L6C2 becomes increasingly congested it starts to restrict the flow that can be sent in from its upstream cell, L6C1. In this manner the congestion jam front propagates backward along the corridor, which can be seen visually from the heatmap. The heatmap shows that the congestion moves down and to the right, with the vertical distance representing how far along the corridor the shockwave travels before being dissipated, and the horizontal distance indicating how long it takes to do so. Notice that the rate at which the wave moves backwards slows down when the demand decreases, because less flow entering a cell means that the density grows less rapidly and takes longer to affect the upstream cell.

To visually compare the network speeds, we generate heatmaps under varying C market penetration rates. Figure 4.9 summarizes these results, where plots (a)-(f) correspond to $p_c = 0.0, 0.2, 0.4, 0.6, 0.8, 1.0$, respectively. In general, we see that the congestion caused by the temporary capacity reduction on L6C3 decreases with higher market penetration. These results are intuitive; the capacity increases at high penetration rates, which means that a temporary capacity reduction has less impact on traffic flow. However, the more interesting case is the transition from $p_c = 0.0$ (plot a) to $p_c = 0.2$ (plot b), as this represents the initial introduction of C vehicles during which capacity decreases. Thinking about

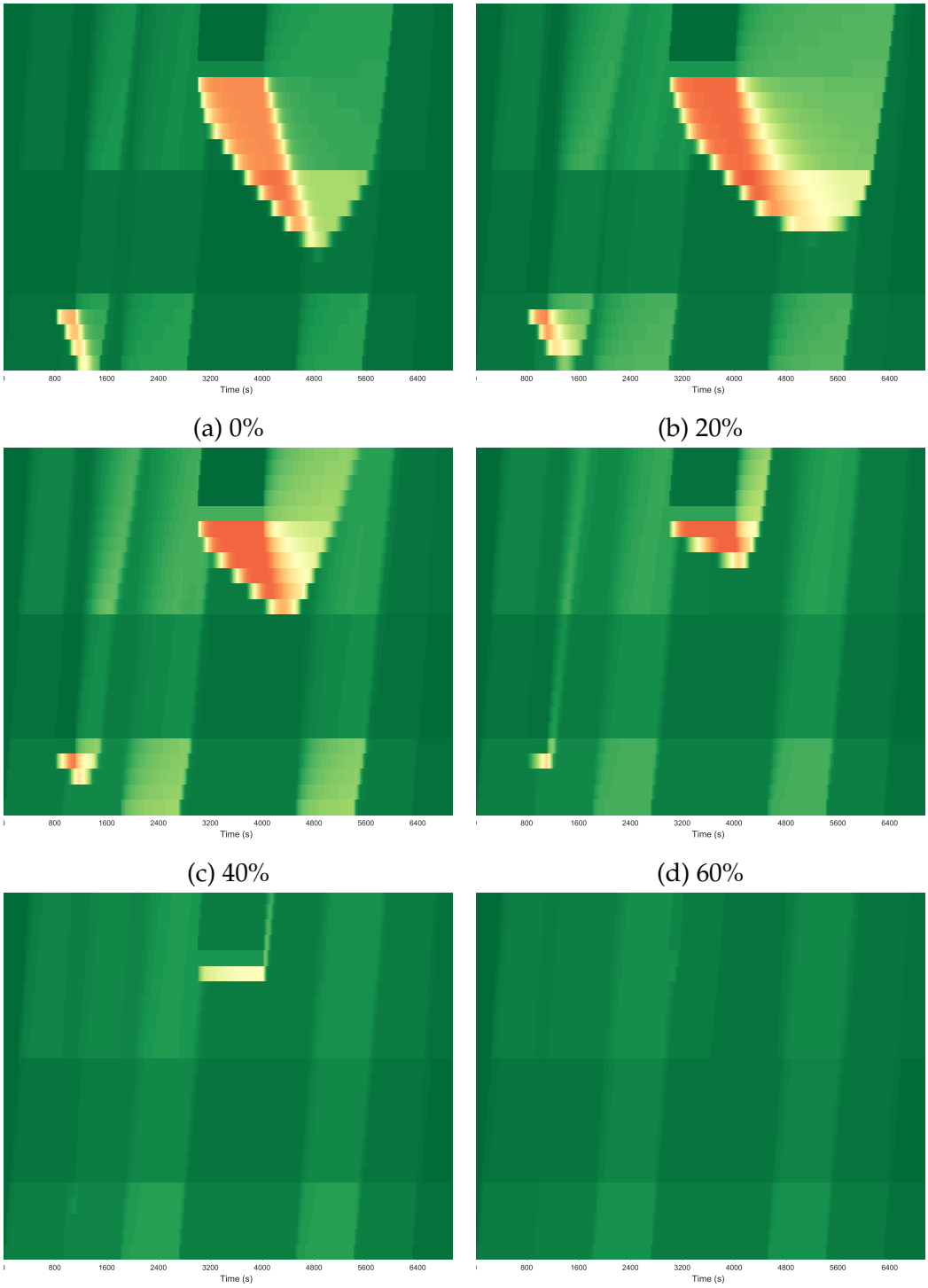

(a) 0%

(b) 20%

(c) 40%

(d) 60%

(e) 80%

(f) 100%

Figure 4.9: Network speeds under varying C market penetration rates.

congestion purely from a capacity perspective, it may seem logical that the congestion pattern should become more pronounced and take longer to dissipate in this transition. However, this interpretation does not consider the shape of the fundamental diagram and how it impacts traffic stability in the vicinity of capacity. In chapter 3 we commented that despite the capacity drop, introducing C vehicles smooths the transition between the uncongested and congested traffic regimes, creating a less dramatic drop in flow and speed relative to the baseline condition with no C vehicles. Judging by the heatmap in subplot (b), we see that this appears to be the case. The backward-moving wave moves upstream more slowly than under the baseline conditions, and dissipates earlier than when there are no C vehicles on the road.

Figure 4.10 shows the fundamental diagrams for $p_c = 0.0$ and $p_c = 0.2$, with dotted lines indicating the abrupt transition between pre and post-incident traffic states. Prior to the incident both traffic states are almost at capacity, and afterwards they drop by 35%. Based on the shape of the curves, it is evident that the slope is more negative for the baseline scenario, which explains why the heat map shows congestion moving upstream more rapidly for $p_c = 0.0$ than for $p_c = 0.2$. These wave speeds are -12.22 mph and -8.87 mph, respectively, and represent the initial backward wave speed (which eventually changes during propagation due to time-varying demand at the system entrance). Notice that in the congested state the density is higher for $p_c = 0.2$ (about 111.5 veh/mi/lane versus 90 veh/mi/lane). This indicates that even with a lower capacity, the curve representing 20% C vehicles is able to accommodate an additional 21.5 veh/mi/lane

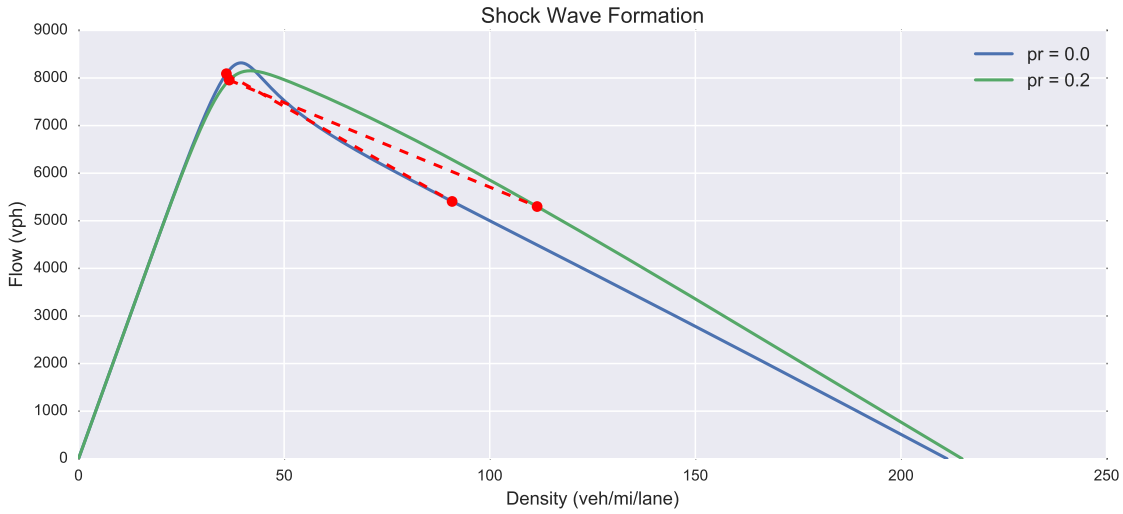

Figure 4.10: Shock wave formation due to incident.

while maintaining the same flow level. The result of this is that each cell can accept more incoming traffic flow before affecting the upstream cell, which slows the backward propagation of the shockwave. When the incident is cleared at t = 4000 on L6C3, another shock wave is sent upstream and overtakes the first wave. Due to the fact that the initial jam front moves backward at a slower speed when $p_c = 0.2$, the second wave is able to overtake it and dissipate the wave farther downstream (i.e., closer to the incident).

In summary, this simulation highlights two factors that impact traffic flow: capacity and the shape of the fundamental diagram. The impact of capacity is straightforward; higher capacity corresponds to higher theoretical throughput and lower volume to capacity ratio for a fixed volume - both of which decrease a system's VHT. However, the shape of the fundamental diagram is also important. A flow-density diagram that peaks sharply at low densities achieves maximum throughput at high speeds, but breaks down quickly when experiencing conges-

tion. This corresponds to decreased VHT when the system is uncongested, but can cause the system to be unstable near capacity when traffic flow enters the congested regime. In contrast, smoother flow-density diagrams correspond to traffic flow dynamics which are less volatile; they have a wider range of traffic densities in which they can sustain volumes near capacity, and do not break down rapidly upon entering a congested regime. Putting these concepts in the context of C market penetration, we see that at penetration rates below 0.4 there is a trade off between capacity and stability. For example, at $p_c = 0.2$, capacity is lower than when $p_c = 0.0$, but the fundamental diagram is smoother and is better able to handle congestion. For penetration rates higher than $p_c = 0.4$ there is no longer a trade off; capacity increases while the fundamental diagram becomes increasingly smooth (i.e., less volatile and subject to quick transitions when exceeding the critical density).

Chapter 5: Conclusions

In response to rapidly advancing automated and connected vehicle technology, this paper presents a framework for describing the equilibrium impact of cooperative adaptive cruise control (C) vehicles on traffic flow. In particular, it focuses on the phase-in period when traffic is composed of both standard (S) and C vehicles, describing how C market penetration affects capacity and traffic performance in a single lane, and extending the modeling framework for network-level analysis under varying demand levels and market penetration rates. Relative to previous work that tends to focus on capacity analysis or use microsimulation to generate aggregate results, this macroscopic modeling framework analytically considers how market penetration and distribution assumptions impact aggregate fundamental traffic relations. Thus, it captures heterogeneous microscopic car-following behavior at a macroscopic level under steady state conditions, which is much more tractable for large-scale analysis and planning applications.

The experimental results suggest that C vehicles may initially cause the overall lane capacity to decrease as they are introduced to a homogeneous traffic stream of standard vehicles, but eventually improve significantly at high market

penetration. Furthermore, even at low market penetration, C vehicles may help stabilize traffic by slowing congestion propagation due to the shape of the fundamental diagram. Although these results show that the critical point at which capacity begins improving is around 40% C vehicles, this point depends on the specific implementation of ACC and V2V technology and the existing driver population.

5.1 Extensions and Future Work

The line of research proposed in this thesis can be extended in a number of different directions, either by expanding the scope or addressing assumptions made in the paper. A few particularly interesting extensions include:

1. *Dedicated Lanes* Given the ability to quantify aggregate traffic characteristics for arbitrary mixes of standard and connected vehicles, a natural question that arises is whether it is advantageous to restrict access on some lanes to only C vehicles. Assuming there is no dynamic control strategy to optimize the vehicle allocation and that C vehicles can choose between general purpose lanes or dedicated C lanes depending on system performance, C vehicles will likely distribute themselves between both facilities in a User Equilibrium manner (i.e., where either all C vehicles travel on the C-only lane if it has better performance, or both the general purpose and C-only lanes have the same experienced travel time). In light of this, it would be interesting to analyze how the presence of dedicated lanes might impact

the total system cost. That is, given that all drivers behave according to UE driving strategies, does simply limiting access to certain lanes improve the overall system performance? If so, how many lanes should be allocated to C vehicles, and under what demand and market penetration rates does this hold?

2. *Managed Lanes* Rather than imposing access restrictions on particular lanes, it would be interesting to explore the extent to which system performance could be improved through dynamic lane management strategies. To assess the value of this, we could model a setup similar to the one described for dedicated lanes, but relax the UE assumption. Instead of assuming that C vehicles allocate themselves such that no driver can improve their travel time, we could solve an optimization problem to determine the system optimal allocation. If there is significant value to trying to shift the allocation from UE to System Optimal Equilibrium (SOE), a dynamic control strategy (e.g., dynamic pricing) could be employed to try to encourage the optimal number of C vehicles on the managed lane. Further research could explore whether it is ever worth giving standard vehicles an opportunity to pay for improved performance and join a lane typically reserved for C vehicles (analogous to High Occupancy Toll lanes).

3. *Network Development* This modeling approach can be utilized in a network-level optimization framework to determine where and when to best introduce C vehicles (or managed/dedicated lane infrastructure) onto a road

network. Specifically, the first order macroscopic model can be used to quantify traffic conditions and thus compute performance metrics that are used in the objective function.

4. *Impact of Platoons* This thesis captures the arrangement of C vehicles on a lane through parameter A, which describes whether vehicle classes are randomly mixed or completely separated. The analysis showed that performance improves when vehicle classes are separated, so it may be advantageous to impose some type of control measures to form platoons of connected vehicles, and treat them as a group instead of individual vehicles. For example, if C vehicles were able to platoon in all lanes, the optimal lane allocation problem considered in this paper would likely involve deciding how to allocate groups of standard and connected vehicles amongst lanes.

5. *Microsimulation modeling framework* Although this thesis focused on the macroscopic aspects of mixed standard and connected vehicle traffic, the LCM framework may be used to investigate microscopic car-following properties. In particular, it would be beneficial to compare the steady state curves derived analytically in this paper to ones obtained through microsimulation using the same LCM car-following model and assumptions. Modeling at the microscopic level would also allow for additional analyses, including investigation of local and string stability, and vehicle-level control applications.

While these extensions provide rich opportunities to further extend the literature, this thesis provides an important foundation for such research. By proposing a cooperative adaptive cruise control vehicle modeling framework, analyzing traffic flow impact on single and multiple lane roads, and quantifying optimal lane allocation strategies at the link level under varying demand and C market penetration, this thesis takes an important initial step in quantifying the impact of a potentially disruptive technology.

References

Askari, A., Farias, D. A., Kurzhanskiy, A. A., and Varaiya, P. (2016). Measuring impact of adaptive and cooperative adaptive cruise control on throughput of signalized intersections. *arXiv preprint arXiv:1611.08973*.

Bando, M., Hasebe, K., Nakanishi, K., Nakayama, A., Shibata, A., and Sugiyama, Y. (1995a). Phenomenological study of dynamical model of traffic flow. *Journal de Physique I*, 5(11):1389–1399.

Bando, M., Hasebe, K., Nakayama, A., Shibata, A., and Sugiyama, Y. (1994). Structure stability of congestion in traffic dynamics. *Japan Journal of Industrial and Applied Mathematics*, 11(2):203–223.

Bando, M., Hasebe, K., Nakayama, A., Shibata, A., and Sugiyama, Y. (1995b). Dynamical model of traffic congestion and numerical simulation. *Physical review E*, 51(2):1035.

Becker, J. C. and Simon, A. (2000). Sensor and navigation data fusion for an autonomous vehicle. In *Intelligent Vehicles Symposium, 2000. IV 2000. Proceedings of the IEEE*, pages 156–161. IEEE.

Bose, A. and Ioannou, P. (2003). Mixed manual/semi-automated traffic: A macroscopic analysis. *Transportation Research Part C: Emerging Technologies*, 11(6):439–462.

Buehler, M., Iagnemma, K., and Singh, S. (2009). *The DARPA urban challenge: Autonomous vehicles in city traffic*, volume 56. springer.

Chandler, R. E., Herman, R., and Montroll, E. W. (1958). Traffic dynamics: Studies in car following. *Operations research*, 6(2):165–184.

Chen, J., Liu, R., Ngoduy, D., and Shi, Z. (2016). A new multi-anticipative car-following model with consideration of the desired following distance. *Nonlinear Dynamics*, 85(4):2705–2717.

Chen, X., Li, R., Xie, W., and Shi, Q. (2009). Stabilization of traffic flow based on multi-anticipative intelligent driver model. In *Intelligent Transportation Systems, 2009. ITSC'09. 12th International IEEE Conference on*, pages 1–6. IEEE.

Cheng, L., Henty, B. E., Stancil, D. D., Bai, F., and Mudalige, P. (2007). Mobile vehicle-to-vehicle narrow-band channel measurement and characterization of the 5.9 ghz dedicated short range communication (DSRC) frequency band. *IEEE Journal on Selected Areas in Communications*, 25(8).

Courant, R., Friedrichs, K., and Lewy, H. (1967). On the partial difference equations of mathematical physics. *IBM journal*, 11(2):215–234.

Daganzo, C. F. (1994). The cell transmission model: A dynamic representation of highway traffic consistent with the hydrodynamic theory. *Transportation Research Part B: Methodological*, 28(4):269–287.

Darbha, S. and Rajagopal, K. (1999). Intelligent cruise control systems and traffic flow stability. *Transportation Research Part C: Emerging Technologies*, 7(6):329–352.

Davis, L. (2004). Effect of adaptive cruise control systems on traffic flow. *Physical Review E*, 69(6):066110.

Davis, L. (2007). Effect of adaptive cruise control systems on mixed traffic flow near an on-ramp. *Physica A: Statistical Mechanics and its Applications*, 379(1):274–290.

Delis, A. I., Nikolos, I. K., and Papageorgiou, M. (2016). Simulation of the penetration rate effects of ACC and CACC on macroscopic traffic dynamics. In *Intelligent Transportation Systems (ITSC), 2016 IEEE 19th International Conference on*, pages 336–341. IEEE.

Diakaki, C., Papageorgiou, M., Papamichail, I., and Nikolos, I. (2015). Overview and analysis of vehicle automation and communication systems from a motorway traffic management perspective. *Transportation Research Part A: Policy and Practice*, 75:147–165.

Fagnant, D. J. and Kockelman, K. (2015). Preparing a nation for autonomous vehicles: Opportunities, barriers and policy recommendations. *Transportation Research Part A: Policy and Practice*, 77:167–181.

Farhi, N. (2012). Piecewise linear car-following modeling. *Transportation Research Part C: Emerging Technologies*, 25:100–112.

Forbes, T. (1963). Human factor considerations in traffic flow theory. *Highway Research Record*, (15).

Gipps, P. G. (1981). A behavioural car-following model for computer simulation. *Transportation Research Part B: Methodological*, 15(2):105–111.

Goodall, N. (2014). Ethical decision making during automated vehicle crashes. *Transportation Research Record: Journal of the Transportation Research Board*, (2424):58–65.

Greenshields, B. D., Thompson, J., Dickinson, H., and Swinton, R. (1934). The photographic method of studying traffic behavior. In *Highway Research Board Proceedings*, volume 13.

Hall, D. L. and Llinas, J. (2001). Multisensor data fusion. In *Multisensor Data Fusion*. CRC press.

Horiguchi, R. and Oguchi, T. (2014). A study on car following models simulating various adaptive cruise control behaviors. *International Journal of Intelligent Transportation Systems Research*, 12(3):127–134.

Hu, J., Kong, L., Shu, W., and Wu, M.-Y. (2012). Scheduling of connected autonomous vehicles on highway lanes. In *Global Communications Conference (GLOBECOM), 2012 IEEE*, pages 5556–5561. IEEE.

Hussain, O., Ghiasi, A., Li, X., and Qian, Z. (2016). Freeway lane management approach in mixed traffic environment with connected autonomous vehicles. *arXiv preprint arXiv:1609.02946*.

Jerbi, M., Marlier, P., and Senouci, S. M. (2007). Experimental assessment of V2V and I2V communications. In *Mobile Adhoc and Sensor Systems, 2007. MASS 2007. IEEE International Conference on*, pages 1–6. IEEE.

Jiang, D., Taliwal, V., Meier, A., Holfelder, W., and Herrtwich, R. (2006). Design of 5.9 GHz DSRC-based vehicular safety communication. *IEEE Wireless Communications*, 13(5).

Jin, P., Yang, D., Ran, B., Cebelak, M., and Walton, C. (2013). Bidirectional control characteristics of general motors and optimal velocity car-following models: Implications for coordinated driving in a connected vehicle environment. *Transportation Research Record: Journal of the Transportation Research Board*, (2381):110–119.

Kammel, S., Ziegler, J., Pitzer, B., Werling, M., Gindele, T., Jagzent, D., Schröder, J., Thuy, M., Goebl, M., Hundelshausen, F. v., et al. (2008). Team AnnieWAY's autonomous system for the 2007 DARPA urban challenge. *Journal of Field Robotics*, 25(9):615–639.

Kesting, A. and Treiber, M. (2008). How reaction time, update time, and adaptation time influence the stability of traffic flow. *Computer-Aided Civil and Infrastructure Engineering*, 23(2):125–137.

Kesting, A., Treiber, M., Schönhof, M., and Helbing, D. (2008). Adaptive cruise control design for active congestion avoidance. *Transportation Research Part C: Emerging Technologies*, 16(6):668–683.

Kesting, A., Treiber, M., Schönhof, M., Kranke, F., and Helbing, D. (2007). Jam-avoiding adaptive cruise control (ACC) and its impact on traffic dynamics. In *Traffic and Granular FlowâĂŹ05*, pages 633–643. Springer.

Kometani, E. and Sasaki, T. (1959). Dynamic behaviour of traffic with a non-linear spacing-speed relationship.

Kumfer, W. and Burgess, R. (2015). Investigation into the role of rational ethics in crashes of automated vehicles. *Transportation Research Record: Journal of the Transportation Research Board*, (2489):130–136.

Labuhn, P. I. and Chundrlik Jr, W. J. (1995). Adaptive cruise control. US Patent 5,454,442.

Lari, A., Douma, F., and Onyiah, I. (2015). Self-driving vehicles and policy implications: Current status of autonomous vehicle development and minnesota policy implications. *Minn. JL Sci. & Tech.*, 16:735.

Lenz, H., Wagner, C., and Sollacher, R. (1999). Multi-anticipative car-following model. *The European Physical Journal B-Condensed Matter and Complex Systems*, 7(2):331–335.

Levin, M. W. and Boyles, S. D. (2016). A multiclass cell transmission model for shared human and autonomous vehicle roads. *Transportation Research Part C: Emerging Technologies*, 62:103–116.

Li, Y., Zhang, L., Peeta, S., He, X., Zheng, T., and Li, Y. (2016). A car-following model considering the effect of electronic throttle opening angle under connected environment. *Nonlinear Dynamics*, 85(4):2115–2125.

Liang, C.-Y. and Peng, H. (1999). Optimal adaptive cruise control with guaranteed string stability. *Vehicle system dynamics*, 32(4-5):313–330.

Lighthill, M. J. and Whitham, G. B. (1955). On kinematic waves. II. A theory of traffic flow on long crowded roads. In *Proceedings of the Royal Society of London A: Mathematical, Physical and Engineering Sciences*, volume 229, pages 317–345. The Royal Society.

Logghe, S. and Immers, L. H. (2008). Multi-class kinematic wave theory of traffic flow. *Transportation Research Part B: Methodological*, 42(6):523–541.

Mahmassani, H. S. (2016). 50th anniversary invited article - Autonomous vehicles and connected vehicle systems: Flow and operations considerations. *Transportation Science*, 50(4):1140–1162.

Marsden, G., McDonald, M., and Brackstone, M. (2001). Towards an understanding of adaptive cruise control. *Transportation Research Part C: Emerging Technologies*, 9(1):33–51.

Milanés, V. and Shladover, S. E. (2014). Modeling cooperative and autonomous adaptive cruise control dynamic responses using experimental data. *Transportation Research Part C: Emerging Technologies*, 48:285–300.

Mitchell, J. S., Payton, D. W., and Keirsey, D. M. (1987). Planning and reasoning for autonomous vehicle control. *International Journal of Intelligent Systems*, 2(2):129–198.

Montemerlo, M., Becker, J., Bhat, S., Dahlkamp, H., Dolgov, D., Ettinger, S., Haehnel, D., Hilden, T., Hoffmann, G., Huhnke, B., et al. (2008). Junior: The Stanford entry in the urban challenge. *Journal of field Robotics*, 25(9):569–597.

Ngoduy, D. (2012). Application of gas-kinetic theory to modelling mixed traffic of manual and ACC vehicles. *Transportmetrica*, 8(1):43–60.

Ngoduy, D. (2013). Instability of cooperative adaptive cruise control traffic flow: A macroscopic approach. *Communications in Nonlinear Science and Numerical Simulation*, 18(10):2838–2851.

Ngoduy, D. and Jia, D. (2016). Multi anticipative bidirectional macroscopic traffic model considering cooperative driving strategy. *Transportmetrica B: Transport Dynamics*, pages 1–15.

NHTSA (2011). USDOT connected vehicle research program: Vehicle-to-vehicle safety application research plan. Technical report.

Ni, D. (2015). *Traffic flow theory: Characteristics, experimental methods, and numerical techniques*. Butterworth-Heinemann.

Ni, D., Leonard, J. D., Jia, C., and Wang, J. (2015). Vehicle longitudinal control and traffic stream modeling. *Transportation Science*, 50(3):1016–1031.

Nikolos, I. K., Delis, A. I., and Papageorgiou, M. (2015). Macroscopic modelling and simulation of acc and cacc traffic. In *Intelligent Transportation Systems (ITSC), 2015 IEEE 18th International Conference on*, pages 2129–2134. IEEE.

Nowakowski, C., O'Connell, J., Shladover, S. E., and Cody, D. (2010). Cooperative adaptive cruise control: Driver acceptance of following gap settings less than one second. In *Proceedings of the Human Factors and Ergonomics Society Annual Meeting*, volume 54, pages 2033–2037. SAGE Publications Sage CA: Los Angeles, CA.

Ntousakis, I. A., Nikolos, I. K., and Papageorgiou, M. (2015). On microscopic modelling of adaptive cruise control systems. *Transportation Research Procedia*, 6:111–127.

Papageorgiou, M., Papamichail, I., Messmer, A., and Wang, Y. (2010). Traffic simulation with metanet. In *Fundamentals of traffic simulation*, pages 399–430. Springer.

Pilutti, T. and Ulsoy, A. G. (1999). Identification of driver state for lane-keeping tasks. *IEEE transactions on systems, man, and cybernetics-Part A: Systems and humans*, 29(5):486–502.

Pipes, L. A. (1953). An operational analysis of traffic dynamics. *Journal of applied physics*, 24(3):274–281.

Pomerleau, D. and Jochem, T. (1996). Rapidly adapting machine vision for automated vehicle steering. *IEEE expert*, 11(2):19–27.

Qian, Z. S., Li, J., Li, X., Zhang, M., and Wang, H. (2017). Modeling heterogeneous traffic flow: A pragmatic approach. *Transportation Research Part B: Methodological*, 99:183–204.

Richards, P. I. (1956). Shock waves on the highway. *Operations research*, 4(1):42–51.

Risack, R., Mohler, N., and Enkelmann, W. (2000). A video-based lane keeping assistant. In *Intelligent Vehicles Symposium, 2000. IV 2000. Proceedings of the IEEE*, pages 356–361. IEEE.

Schakel, W. J., Van Arem, B., and Netten, B. D. (2010). Effects of cooperative adaptive cruise control on traffic flow stability. In *Intelligent Transportation Systems (ITSC), 2010 13th International IEEE Conference on*, pages 759–764. IEEE.

Shladover, S., Su, D., and Lu, X.-Y. (2012). Impacts of cooperative adaptive cruise control on freeway traffic flow. *Transportation Research Record: Journal of the Transportation Research Board*, (2324):63–70.

Subramanian, V., Burks, T. F., and Arroyo, A. (2006). Development of machine vision and laser radar based autonomous vehicle guidance systems for citrus grove navigation. *Computers and electronics in agriculture*, 53(2):130–143.

Sugiyama, Y. (1999). Optimal velocity model for traffic flow. *Computer Physics Communications*, 121:399–401.

Talebpour, A., Mahmassani, H. S., and Bustamante, F. E. (2016). Modeling driver behavior in a connected environment: Integrated microscopic simulation of traffic and mobile wireless telecommunication systems. *Transportation Research Record: Journal of the Transportation Research Board*, (2560):75–86.

Taliwal, V., Jiang, D., Mangold, H., Chen, C., and Sengupta, R. (2004). Empirical determination of channel characteristics for DSRC vehicle-to-vehicle communication. In *Proceedings of the 1st ACM international workshop on Vehicular ad hoc networks*, pages 88–88. ACM.

Treiber, M. and Helbing, D. (2001). Microsimulations of freeway traffic including control measures. *Automatisierungstechnik. Vol. 49, no. 11*.

Treiber, M., Hennecke, A., and Helbing, D. (2000). Congested traffic states in empirical observations and microscopic simulations. *Physical review E*, 62(2):1805.

Treiber, M. and Kesting, A. (2013). *Traffic Flow Dynamics: Data, Models and Simulation*.

Vahidi, A. and Eskandarian, A. (2003). Research advances in intelligent collision avoidance and adaptive cruise control. *IEEE transactions on intelligent transportation systems*, 4(3):143–153.

Van Arem, B., Hogema, J., Vanderschuren, M., and Verheul, C. (1996). An assessment of the impact of autonomous intelligent cruise control.

Van Arem, B., Van Driel, C. J., and Visser, R. (2006). The impact of cooperative adaptive cruise control on traffic-flow characteristics. *IEEE Transactions on Intelligent Transportation Systems*, 7(4):429–436.

VanderWerf, J., Shladover, S., Kourjanskaia, N., Miller, M., and Krishnan, H. (2001). Modeling effects of driver control assistance systems on traffic. *Transportation Research Record: Journal of the Transportation Research Board*, (1748):167–174.

Wang, J. and Rajamani, R. (2004). Should adaptive cruise-control systems be designed to maintain a constant time gap between vehicles? *IEEE Transactions on Vehicular Technology*, 53(5):1480–1490.

Wilson, R., Berg, P., Hooper, S., and Lunt, G. (2004). Many-neighbour interaction and non-locality in traffic models. *The European Physical Journal B-Condensed Matter and Complex Systems*, 39(3):397–408.

Wong, G. and Wong, S. (2002). A multi-class traffic flow model - an extension of LWR model with heterogeneous drivers. *Transportation Research Part A: Policy and Practice*, 36(9):827–841.

Xu, Q., Mak, T., Ko, J., and Sengupta, R. (2004). Vehicle-to-vehicle safety messaging in DSRC. In *Proceedings of the 1st ACM international workshop on Vehicular ad hoc networks*, pages 19–28. ACM.

Ye, F., Adams, M., and Roy, S. (2008). V2V wireless communication protocol for rear-end collision avoidance on highways. In *Communications Workshops, 2008. ICC Workshops' 08. IEEE International Conference on*, pages 375–379. IEEE.

Yi, J. and Horowitz, R. (2006). Macroscopic traffic flow propagation stability for adaptive cruise controlled vehicles. *Transportation Research Part C: Emerging Technologies*, 14(2):81–95.

Yokota, T. K. (1998). A study of AHS effects on traffic flow at bottlenecks. In *Towards the new horizon together. Proceedings of the 5th world congress on intelligent transport systems, held 12-16 October 1998, Seoul, Korea, paper no. 3200*.

Zheng, L., Jin, P. J., and Huang, H. (2015). An anisotropic continuum model considering bi-directional information impact. *Transportation Research Part B: Methodological*, 75:36–57.

Zheng, L., Ma, S., and Zhong, S. (2011). Analysis of honk effect on the traffic flow in a cellular automaton model. *Physica A: Statistical Mechanics and its Applications*, 390(6):1072–1084.

Zwaneveld, P. J. and Van Arem, B. (1997). Traffic effects of automated vehicle guidance systems: a literature survey.